River suspended-sand flux computation with uncertainty estimation, using water samples and high-resolution ADCP measurements

Laible Jessica[1,*], Dramais Guillaume[1,*], Le Coz Jérôme[1], Calmel Blaise[1], Camenen Benoît[1], Topping David J.[2], Santini William[3], Pierrefeu Gilles[4], and Lauters François[5]

[1]RiverLy, INRAE, 5 Rue de la Doua, Villeurbanne, 69100, France
[2]U.S. Geological Survey, USGS, 2255 N. Gemini Drive, Flagstaff, AZ 86001, USA
[3]IRD-GET, Institut de Recherche pour le Développement, Laboratoire GET (IRD, CNRS, UPS, CNES), Toulouse, France
[4]CACOH, CNR, 4 Rue de Chalon-sur-Saône, Lyon, 69007, France
[5]Service Etudes Eau Environnement, EDF, 134 Rue de l'étang, Saint Martin Le Vinoux, 38950, France
[*]These authors contributed equally to this work.

Correspondence: Dramais Guillaume (guillaume.dramais@inrae.fr), Jessica Laible (jessica.laible@inrae.fr)

Abstract. Measuring suspended-sand fluxes in rivers remains a scientific challenge due to their high spatial and temporal variability. To capture the vertical and lateral gradients of concentration in the cross section, measurements with point samples are performed. However, the uncertainty related to these measurements is rarely evaluated, as few studies of the major sources of error exist. Therefore, the aim of this study is to develop a method determining the cross sectional sand flux and estimating its

5 uncertainty. This SDC (for Sand Discharge Computing) method combines suspended-sand concentrations from point samples with ADCP (Acoustic Doppler Current Profiler) high-resolution depth and velocity measurements. The MAP (for Multitransect Averaged Profile) method allows to obtain an average of several ADCP transects on a regular grid, including the unmeasured areas. The suspended-sand concentrations are integrated vertically by fitting a theoretical exponential suspended-sand profile to the data using Bayesian modelling. The lateral integration is based on the water depth as a proxy for the local bed shear

10 stress to evaluate the bed concentration and sediment diffusion along the river cross-section to evaluate the bed concentration and sediment diffusion along the river cross-section. The estimation of uncertainty combines ISO standards and semi-empirical methods with a Bayesian approach to estimate the uncertainty due to the vertical integration. The new method is applied to data collected in four rivers under various hydro-sedimentary conditions: the Colorado, Rhône, Isère and Amazon Rivers, with computed flux uncertainties ranging between 18 and 32 %. The relative difference between the suspended-sand flux in

15 21 cases calculated with the proposed SDC method compared to the ISO 4363 method ranges between -16 and +3 %. This method, which comes with a flexible, open-source code, is the first proposing an applicable uncertainty estimation, that could be adapted to other flux computation methods.

1 Introduction

20 The determination of suspended-sediment load is required to estimate sediment dynamics and budgets for river restoration and monitoring, river engineering, and flood risk evaluation (Kondolf et al., 2014). Measuring and monitoring sediment loads and the associated uncertainties within a catchment is a major practical issue for hydrologists and river managers (Hoffmann et al., 2010). Even though suspended-sand transport is a key driver of the river evolution (Kondolf, 1997), it remains difficult to measure its concentration due to its temporal and spatial variability in the cross section (Armijos et al., 2017). In contrast,

25 fine suspended sediments (<63 μm) are relatively homogeneous throughout the cross section (Wren et al., 2000).

The total suspended-sediment flux through a cross section, Φ_{total} (kg s^{-1}), is defined as the mass of suspended-sediment passing through a river cross section per unit time:

$$\Phi_{total} = \int\limits_{y_{\mathrm{lb}}}^{y_{\mathrm{rb}}} q_{\mathrm{ss}}(y)dy = \int\limits_{y_{\mathrm{lb}}}^{y_{\mathrm{rb}}} \int\limits_{z_a}^{h} c(y,z)u(y,z)dzdy \tag{1}$$

where y and z are the lateral and vertical coordinates, q_{ss} is the suspended-sediment discharge per vertical, y_{lb} and y_{rb} are the

30 left and right boundaries of the cross section, z_a is the reference level for suspension at the top of the bedload layer, generally assumed to be the riverbed elevation, h is the water elevation, and $c(z)$ and $u(z)$ are the time-averaged suspended-sediment concentration and the water velocity perpendicular to the cross section, respectively.

Suspended-sediment sampling and computing techniques have been developed over decades (Porterfield, 1972; Starosolsky and Rakoczi, 1981; ISO 4363, 2002). Typically, these methods are based on physical water sampling to determine the suspended

35 sediment concentration throughout the cross section using samples taken at different locations throughout the river cross section. Samples may be taken following the depth-integrating method, where several nearly complete verticals at different distances from the bank are sampled, or the point-sampling method, where samples are collected at different, discrete water depths and distances from the bank. Different methods were proposed to estimate the suspended-sand flux through the cross section (Lupker et al., 2011; Shah-Fairbank and Julien, 2015; Santini et al., 2019). The ISO method (ISO 4363, 2002) consists

40 of computing the velocity-weighted cross sectional mean concentration by combining physical samples with simultaneous velocity measurements. In this method, the cross section is divided into N_{seg} segments and for each increment l, the water discharge Q_l and depth-averaged velocity-weighted concentration C_l are evaluated:

$$\Phi_{\mathrm{total}} = \sum_{l=1}^{N_{\mathrm{seg}}} Q_l \, C_l \tag{2}$$

This method is derived directly from the velocity-area method for the measurement of water discharge using current meters

45 (ISO 748, 2009). Even though these classical, discrete methods are widely accepted, they are time- and cost-consuming and sometimes difficult to deploy (Camenen et al., 2023). As they are limited to a few points or depth-averaged samples at a limited number of locations, they are characterized by a low spatial and temporal resolution. Also, the method is directly based on depth-integrating sampling with no possibility to interpolate and extrapolate results from sampled verticals to the whole cross-section. Some surrogate technologies (e.g. optical and acoustical methods) have been proposed to measure sediment

50 properties and suspended-sand flux with a better spatial and temporal resolution (Wren et al., 2000; Gray and Gartner, 2010).

Acoustic methods using the Acoustic Doppler Current Profilers (ADCP) have become well-established in stream flow monitoring and provide faster, safer and more accurate acquisition of stream velocities, discharges and depths than older current meter methods (Oberg and Mueller, 2007). In a measurement transect, data are acquired on a grid with fixed or variable cell height and many vertical ensembles. For a valid discharge measurement, several cross sectional transects are typically acquired

55   and processed to obtain information on discharge and velocity. Different post-processing tools have been developed such as VMT (Parsons et al., 2013) for the analysis and visualization of cross sectional velocity data collected along multiple ADCP transects. Other examples are QRev (Mueller, 2016) and QRevInt (Lennermark and Hauet, 2022), which are applied to ensure discharge measurement reliability and to quantify the uncertainty in the discharge measurement (Despax et al., 2023).

In combination with sediment sampling, ADCP measurements of flow velocity and depth can be used to compute the cross

60   sectional suspended-sand flux (Bouchez et al., 2011; Vauchel et al., 2017). ADCP measurements provide an increased spatial resolution throughout the cross section compared to point velocity measurements using current meters or rating-curve estimates of the total cross sectional discharge (Oberg and Mueller, 2007). Moreover, the acoustic backscatter measured by an ADCP or an Acoustic Backscattering System (ABS) may be inverted and used to measure the suspended-sand concentration (e.g. Topping and Wright 2016; Venditti et al. 2016; Szupiany et al. 2019; Vergne et al. 2020). Several software tools have been

65   developed to process ADCP data for estimating suspended-sand flux (Boldt, 2015; Dominguez Ruben et al., 2020) or using backscatter inversions. However, acoustic inversion techniques require many physical samples for calibration, and are affected by acoustic modelling issues (Vergne et al., 2023).

Informed decisions related to sediment monitoring require reliable estimates of the uncertainty of flux measurements. However, the evaluation of the uncertainty is a difficult task because of the complexity of these measurements, due mainly to the

70   temporal and spatial variations of the sediment concentration. Measurement uncertainty is the expression of the statistical dispersion of the values attributed to a measured quantity (JCGM, 2008). Identifying error sources and estimating uncertainty components for suspended-sand measurements have been addressed in many old reports and papers from the FISP (Federal Inter-Agency Sedimentation Project)(FISP, 1941, 1952; Colby, 1964; Guy and Norman, 1970) and more recently by the USGS (Topping et al., 2011; Sabol and Topping, 2013) and others (Gitto et al., 2017). Moreover, the ISO 4363 (2002) standard pro-

75   poses a framework to estimate the errors and uncertainty in the mean cross sectional suspended-sand concentration determined by a point-sampling method. It identifies several sources of error, random and systematic ones, that are related to the lateral integration (i.e. the number of verticals), the vertical integration (i.e. the number of sampling points along a vertical), the sampling time (i.e. the natural fluctuation and time-averaging), the sampler and the laboratory analysis. The uncertainty related to each of these error sources is estimated, notably by increasing the sampling number on the point, along the vertical or within

80   the cross section to estimate an approximate true value. The respective uncertainty is then determined by the difference between the measured value at a given location and the approximate true value. Even though several sources of error are addressed, the ISO 4363 (2002) method contains several defects in theoretical and practical aspects. First, this standard is not in agreement with the framework proposed in the Guide to the expression of Uncertainty in Measurement (GUM, JCGM (2008)) defining the uncertainty propagation method, notably concerning the notations and the computation of an approximate true value. Second,

85   the large amount of additional samples required for the uncertainty analysis is not realistic to apply. For example, to estimate

the uncertainty due to the number of verticals (i.e. lateral integration), 15 to 20 verticals with seven point samples each are required for sections less than 100 m wide. The time needed to conduct this kind of survey is practically impossible given the temporal variability of the processes studied.

Besides the ISO 4363 (2002) method, no other method proposes a framework addressing all commonly identified sources

90 of error. However, some authors tried to evaluate the main sources of uncertainty. Concerning lateral integration, Colby (1964) stated that the variability of sand concentration at different sampling verticals should be closely related to the variability of $\overline{v}^2/h$, the ratio of the squared mean velocity $\overline{v}$ to the total sampled depth h. To ensure comparability among different sampling sections and streams, the $\overline{v}^2/h$ - index, also called ξ, may be used :

$$\xi = \frac{\max\left(\overline{v_l}^2/h_l\right)}{\overline{v_z}^2/\overline{h_z}} \tag{3}$$

95 with $\overline{v_l}$ the depth-averaged velocity and water-depth for each increment l, and $\overline{v_z}$ and $\overline{h_z}$ the depth-averaged velocity and water-depth mean values for the cross section. Based on this concept of variability, Guy and Norman (1970) prepared a nomograph that indicates the number of sampling verticals required for a desired maximum acceptable relative standard-uncertainty as a function of the percentage of sand p_s and ξ.

The issue of the appropriate sampling time and the associated time-averaging has been been the subject of several studies.

100 Topping et al. (2011) analyzed the temporal variability in sediment concentration among point samples and estimated the associated uncertainties for depth-integrated measurements. In addition, Gitto et al. (2017) concluded that a 9 to 12 minutes sampling time was required to get a representative point sample because of the temporal variability in sediment concentration.

Common methods to estimate the mean cross sectional suspended-sand concentration and its uncertainty are subject to various limitations such as the interpolation and extrapolation of the suspended-sand concentration towards the river bed and

105 bank, or the impractical feasibility of the ISO 4363 (2002) uncertainty method. Therefore, the first aim of this study is to introduce a method for computing the total suspended-sand flux with a high spatial resolution. That method combines point samples with ADCP measurements using a physically based understanding of suspended-sediment transport processes. A second aim is to provide a method to estimate the uncertainty related to this suspended-sand flux computation. Therefore, the uncertainties related to several sources of error such as the discharge, the lateral and vertical integration and on the determined

110 point concentrations are estimated and combined following the GUM framework.

The proposed method, named SDC (Sand Discharge Computing), is based on the ADCP measurement grid. Data are then combined with point suspended-sand concentration measurements which are interpolated in the whole cross-section with a physically based method (Fig. 1). Uncertainties components and suspended-sand flux are computed for each data set. The method, proposed to estimate the suspended-sand concentration and the uncertainties is first presented in Sec. 2. Then, these

115 methods are applied to measurements in four rivers across the world with different flow and sediment characteristics (Sec. 3). Finally, the methodology and presented results are discussed and new developments to improve the method are suggested in Sec. 4.

We use the following notations:
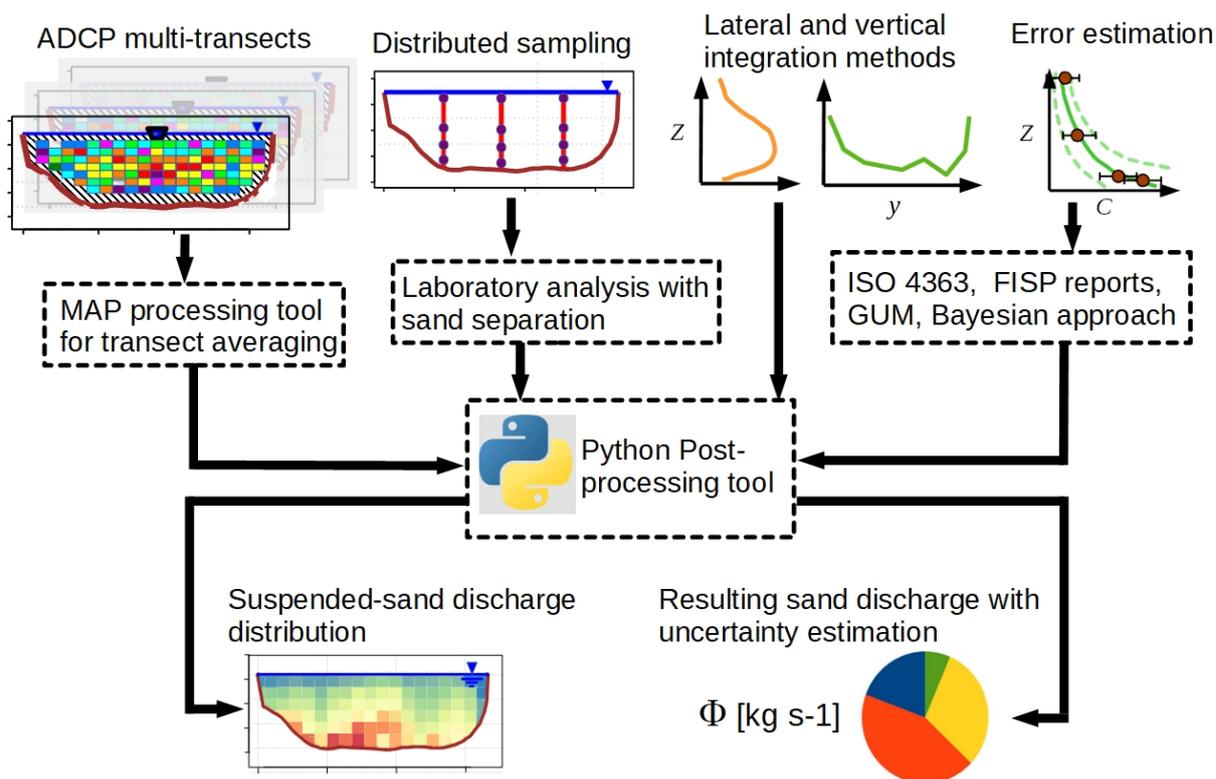
Figure 1. Graphical abstract of the developed SDC method to estimate the suspended-sand flux distribution and the uncertainty in suspended-sand flux through a cross section.

- u is the absolute standard uncertainty, that is, the standard deviation of the probability distribution of errors, "absolute" meaning expressed in the physical unit of the measurement (e.g., in $m^3 \ s^{-1}$ for discharge);

- u' is the relative standard uncertainty, "relative" meaning expressed in % of the measurement;

- $U = ku$ is the absolute expanded uncertainty, with k a coverage factor taken as $k = 2$, which corresponds to a 95 % probability interval if the distribution of errors is Gaussian;

- U' is the relative expanded uncertainty expressed in % of the measurement result.

120

2 Method

2.1 Physically based method to integrate the concentration in the cross section

2.1.1 Creating an ADCP multitransect averaged profile (MAP)

A typical ADCP discharge measurement consists of the average of individual discharge measurements from successive ADCP transects. The Multitransect Averaged Profile (MAP) method aims to include each transect completely to generate an averaged transect profile from the bottom to the water surface including the unmeasured areas. In contrast to VMT (Parsons et al., 2013), the MAP method can compute an average profile in the absence of GPS. This methodology developed with Python is based on the QRevInt (Lennermark and Hauet, 2022) measurement output. QRevInt provides quality analysis and quality control which allows to have clean input data. For each ADCP discharge measurement, composed of several transects, one averaged MAP profile is computed with a regular grid for the whole cross-section (including the unmeasured areas).

First, the MAP method defines a straight average cross section on the selected transects of the measurement. Then, these transects are projected using an orthogonal translation on the average cross section. At this point, each transect is interpolated on the cross section grid. The width and height of cells can be defined by the user. Once each transect is defined on the grid, MAP overlays them to average the basic variables, such as velocity, on each cell. Finally, velocities are extrapolated to unmeasured areas. For the top and the bottom primary velocity extrapolation, MAP uses QRevInt optimized extrapolation law and exponent. As there is no mathematical law for secondary and vertical velocities, they are extrapolated following constant law and linear regression to zero at free-surface and stream-bed respectively. For the extrapolation of the primary velocity to the edges, the MAP method extrapolates the mean velocity of the closest valid vertical following a power law to the bank. Then, it applies the QRevInt optimized power law to each unmeasured vertical in the edge region. Edges extrapolation of secondary velocity uses a linear law between the closest vertical and the edge. Vertical velocity on the edge follows the distribution of vertical velocities on the closest vertical. MAP generates thus a complete averaged profile with homogeneous cell sizes. Each cell contains information on its distance to the left bank, and its depth and velocity components. Primary and secondary velocities are then transformed into stream-wise and cross-stream velocities in order to compute discharge.

2.1.2 Point sampling and laboratory analysis

Each suspended-sediment measurement follows the point-sampling method and contains N_{sub} verticals (typically three to seven) with k samples per vertical (typically four to five). Two types of sampler, a Niskin watertrap-type sampler (instantaneous non-time-averaged sample; Filizola et al. 2009) and isokinetic samplers (US P-06; Spicer 2019) were used in different rivers deployed from boats (Colorado, Rhône and Amazon Rivers) or cable cars (Colorado and Isère Rivers). The target depth is set with a graduated tag line when deploying from the boat or using the depth information from the reel on the cable car. The sampler is equiped with a pressure sensor for post-facto verification (for Rhône, Isère and Amazon Rivers). An electrical valve allows the US P-06 samplers to collect a sample at the desired depth and for the desired sampling duration. For instantaneous samples, taken with the Niskin sampler, a traveler is sent down the rope to close the sampler. For the analysis of the suspended-

sediment concentration of each sample, the standard procedure of the American Society for Testing and Materials (ASTM) option C (ASTM D3977, 2007) is applied, which consists of separating fine sediments and sand by wet sieving, prior to filtration of the fine sediments.

2.1.3 Vertical suspended-sand concentration profiles

160

A physically based method is applied to assign concentrations to individual cells (i, j) in each sampling vertical l. It uses a theoretical vertical suspended-sand concentration profile estimated using a Bayesian approach to interpolate and extrapolate the sand concentrations vertically from point samples. The exponential vertical concentration profile proposed by Camenen and Larson (2008), based on a constant vertical diffusivity ϵ_v throughout the water column, is defined as:

$$C(z) = C_R \exp(\alpha z) \tag{4}$$

165

where $C(z)$ (kg m^{-3} or g l^{-1}) is the sediment concentration at elevation z above the bed, α is the vertical gradient in a logarithmic scale, and C_R is the bottom reference sediment concentration. To estimate the concentration profile $C(z)$, the derived depth-averaged concentration and its uncertainty u'_p due to vertical integration (Sec. 2.2.5), the BaM! method is applied (Mansanarez et al., 2019). The BaM! method is based on Bayesian inference, which allows the computation of the posterior probability of a model's parameters from their prior probability and from observations. The model can then be applied to predict the distribution of a new, unobserved data point. The posterior distribution of the parameters is computed using Bayes theorem, and a large number (> 10,000) of realizations are sampled using an adaptive block Metropolis Markov Chain Monte Carlo (MCMC) sampler (Renard et al., 2006). A linear model is applied using logarithmic concentrations in milligram per liter based on Eq. 4:

170

$$\ln(C(z)) = \ln(C_R) - \alpha z. \tag{5}$$

175

The BaM! simulator produces 500 realizations $\ln(C_n(z))$ of the vertical concentration profile. The MaxPost profile $\ln(C_{n_0}(z))$ used for calculating the sand discharge is computed with the realization of parameters n_0 that maximizes the posterior distribution. From this MaxPost profile, the concentration $C_{i,j}$ in each cell (i, j) along vertical l can be determined. The MaxPost parameters $\ln(C_{R,n_0})$ and α_{n_0} are retained and used for the lateral interpolation (Sec. 2.1.4).

BaM! requires the definition of the prior distribution of the equation parameters, that are here $\ln(C_R)$ and α. Both α and
180
C_R are strictly positive, therefore they are assumed to follow log-normal distributions with parameters μ and σ. Consequently, $\ln(C_R)$ is assumed to follow a Gaussian distribution. The parameters μ_α and σ_α describing the prior distribution of α are the mean and standard deviation of the variable's natural logarithm, respectively. The expected values of α and C_R are evaluated based on local hydro-sedimentary parameters (Camenen and Larson, 2008). The expected value of C_R is calculated using the
185
expression of Camenen and Larson (2008), which is a function of the sedimentological diameter D_*, the Shields parameter θ and the critical bed shear stress θ_{cr}:

$$C_R = 1.5 \, 10^{-3} \, \theta \, \exp(-0.2 \, D_*) \, \exp\left(-4.5 \, \frac{\theta_{cr}}{\theta}\right) \tag{6}$$

The sedimentological diameter, or dimensionless grain size, D_* is calculated as:

$$D_* = \overline{D_{50}} \left(\frac{(s-1)\,g}{\nu^2} \right)^{1/3} \qquad (7)$$

190 where $\overline{D_{50}}$ is the median diameter of the sand suspension averaged over the analyzed vertical, $s = 2.65$ is the relative sediment density, $g = 9.81$ m s^{-2} is the acceleration due to gravity and $\nu \approx 10^{-6}$ m^2 s^{-1} is the kinematic viscosity of water. The expected value of the prior distribution is then converted to $\ln(C_R)$. Similarly, the expected value of α can be determined as (Camenen and Larson, 2008):

$$\alpha = -\frac{6\,w_s}{\sigma_t\,\kappa\,v_*\,h} \qquad (8)$$

195 where w_s (m s^{-1}) is the settling velocity estimated following the formula of Soulsby et al. (1997), σ_t is the turbulent Schmidt number, set equal to 1 as a first approximation, $\kappa = 0.41$ is the von Kármán constant, v_* is the total shear velocity and h is the water depth. Defining the prior of α as a log-normal ensures that it remains negative under all hydro-sedimentary conditions. This implies that concentration decreases as a function of z away from the bed, thereby corresponding to Rouse mechanics for suspended-sediment computing (Rouse, 1937). The concentration of the finest sizes in suspension may increase away from the

200 bed when the concentration of suspended sediment is relatively high due to 'squeezing' effect or density stratification (Hunt, 1969; McLean, 1992) leading to possible positive α-values. We neglect these effects since we focus on sand with relatively low concentrations. Grain size information on vertical l is necessary to determine Eq. 6 and the settling velocity w_s, thus to estimate both $\ln(C_R)$ and α. In case they are not available, no prior parameters are defined and the model is fitted by BaM! on the observations only.

205 The second parameter σ_α of the log-normal distribution of α can be estimated by uncertainty propagation equations established following the Guide to the expression of Uncertainty in Measurement (GUM, JCGM (2008)). It is estimated based on the relative uncertainty u'_α of alpha, supposing $\sigma_\alpha = u'_\alpha$. This approximation works well for small values (< 0.5) of σ of the respective log-normal distribution. The parameter $\sigma_\alpha = u'_\alpha$ is estimated by propagation from Eq. 8:

$$u'_\alpha = \sqrt{u'^2_{ws} + u'^2_{\sigma t} + u'^2_\kappa + u'^2_{v*} + u'^2_h}, \qquad (9)$$

210 Based on expert knowledge and literature, we define the uncertainty in the settling velocity $u'_{ws} = 5\%$ (Camenen, 2007), the uncertainty in the turbulent Schmidt number $u'_{\sigma t} = 20\%$ (Gualtieri et al., 2017), $u'_\kappa = 0$ (theoretical value with negligible variations Smart (2022)), the uncertainty in the shear velocity $u'_{v*} = 5\%$ (Perret et al., 2023) and the uncertainty in the elevation of the sampled point within the water column $u'_h = 5\%$ (Dramais, 2020). With these values, we obtain $u'_\alpha = \sqrt{0.0475} \approx 21.8\%$.

The second parameter $\sigma_{\ln(C_R)}$, the standard deviation of $\ln(C_R)$, could also be determined by an uncertainty propagation

215 derived from the Data Reduction Equation of C_R (Eq. 6). However, it has been shown that the highest uncertainty is related to the structural uncertainty of the formula of C_R itself, not to its parametric uncertainty (Camenen et al., 2014). Indeed, the dataset used to establish the semi-empirical formula of Camenen and Larson (2008) is characterized by a large scatter, with differences of about 50 % between the measured and predicted concentration (other formulas also come with large structural uncertainty). Consequently, it is assumed that $\sigma_{\ln(C_R)} = u'_{C_R} = 50\%$.

2.1.4 Lateral interpolation

The lateral interpolation of the suspended-sand concentration to calculate $C_{i,j}$ in every cell of the MAP-grid is based on a physical approach using the water depth as an index. Following Camenen and Larson (2008), C_R is set proportional to the local bed shear stress, which can be assumed to be proportional to the water depth h, if the friction slope is constant throughout the river cross section (Khodashenas and Paquier, 1999; Camenen et al., 2011). Thus, the ratio $C_{R,j}/h_j$ for each column j in the MAP-grid is estimated through linear interpolation along the cross section. As a first approximation, α_j is assumed independent of the local bed shear stress, since it is mostly influenced by large scale turbulence structures (Van Rijn, 1984). α_j varies linearly with horizontal distance between two adjacent sampling verticals (where α was estimated from the concentration profiles fitted to the samples), and remains constant between the first/last sampling vertical and the edge of the cross section.

2.1.5 Determination of concentration $C_{i,j}$ in each MAP-cell (i,j)

The proposed SDC method is based on the discretization of the river cross section by a regular grid fitted on the ADCP data (MAP-grid) composed of N_j columns and N_i depth cells. The general idea is to assign a concentration and discharge to each cell, so that a flux per cell can be obtained after multiplication. The total cross sectional sand flux Φ_{total} is calculated by summing up the suspended sand fluxes per cell:

$$\Phi_{\text{total}} = \sum_{i=1}^{N_i} \sum_{j=1}^{N_j} \Phi_{i,j} \tag{10}$$

where $\Phi_{i,j}$ (kg s^{-1}) is the suspended-sand flux through one MAP cell i,j. The suspended-sand flux $\Phi_{i,j}$ can be calculated as:

$$\Phi_{i,j} = C_{i,j} Q_{i,j} = C_{i,j} u_{i,j} w_j h_{i,j} \tag{11}$$

where $C_{i,j}$ (kg m^{-3} or g l^{-1}) and $Q_{i,j}$ (m^3 s^{-1}) are the suspended-sand concentration and liquid discharge through each cell (i,j), respectively, $u_{i,j}$ (m s^{-1}) is the normal velocity component, w_j (m) is the width, $h_{i,j}$ (m) is the height of the ith vertical cell in the jth column in the MAP-grid. The discharge $Q_{i,j}$ through each cell is determined using the novel MAP-method based on QRevInt (Lennermark and Hauet, 2022) and the suspended-sand concentration $C_{i,j}$ is determined following the novel, physically based SDC method.

The parameters α and C_R are evaluated for each MAP-cell (i,j) applying the presented vertical and lateral integration. The suspended-sand concentration in each cell in the MAP grid is thus evaluated as:

$$C_{i,j} = \frac{1}{h} \int_{z_{i,j}-h_{i,j}/2}^{z_{i,j}+h_{i,j}/2} C_{R,j} \exp(\alpha_j z) dz \tag{12}$$

2.2 Estimation of the uncertainty in measurements of suspended-sand flux through a cross section

2.2.1 General method

The uncertainty U'_Φ in measurements of the suspended-sand flux through a cross section is based on the calculation of suspended-sand flux (i.e. Eq. 2). Therefore, the flux Φ is the product of discharge Q and mean cross-sectional concentra-
250 tion $\overline{C}$: $\Phi = Q \times \overline{C}$. Thus, U'_Φ can be separated into a factor related to discharge U'_Q and one related to the concentration U'_C:

$$U'_\Phi = \sqrt{{U'_Q}^2 + {U'_C}^2} \qquad (13)$$

Equation (13) is based on the hypothesis that the errors in Q and C are independent, otherwise, the term has to include the associated covariances. Even though a simplification, the assumption that the errors are independent is reasonable, as discharge
255 and concentration are measured independently. To approximate the uncertainty U'_Φ in the suspended-sand flux through a cross section, both uncertainties U'_Q and U'_C on the discharge and concentration have to be determined (Fig. 2).
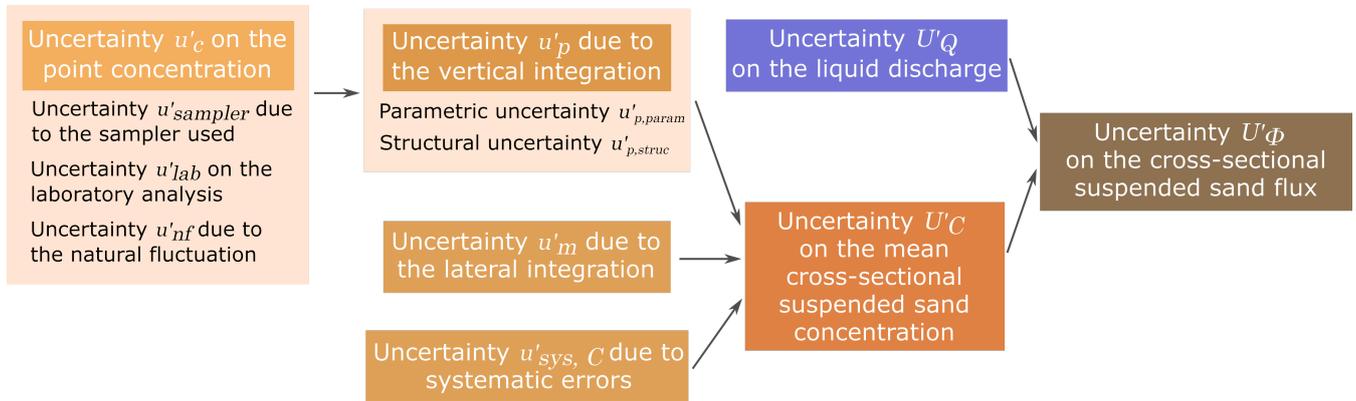
Figure 2. Flow diagram of the developed approach to estimate the uncertainty U'_Φ in the cross sectional suspended-sand flux.

The uncertainty U'_Q in multiple-transect ADCP discharge measurements is calculated following the OURSIN-method (Despax et al., 2023) as implemented in the open-source software QRevInt (Lennermark and Hauet, 2022). U'_C is the combination of several uncertainty components (cf. Fig. 2) listed in Table 1 and detailed afterwards.

260 ### 2.2.2 Uncertainty U'_C in the mean cross sectional suspended-sand concentration

The uncertainty u'^2_C in the mean cross-sectional suspended-sand concentration is calculated as:

$$u'^2_C = u'^2_{\text{sys,C}} + u'^2_m + \sum_{l=1}^{m} \frac{\Phi_l^2}{\Phi^2} u'^2_{p,l}, \qquad (14)$$

Table 1. Uncertainty components used to compute the uncertainty U'_C on the mean cross-sectional suspended sand concentration.

Error sources	Notation (standard uncertainty)	Nature	Estimation method
Lateral interpolation	u_m	Systematic	Nomograph from Guy and Norman (1970)
Vertical interpolation	u_p	Random	Bayesian approach (Sec. 2.2.5): total uncertainty combining the next two components
Vertical interpolation	$u_{p,param}$	Random	Bayesian approach (Sec. 2.2.5): parametric uncertainty
Vertical interpolation	$u_{p,struc}$	Random	Bayesian approach (Sec. 2.2.5): structural uncertainty
Concentration measurements	u_{meas}	Random	Formula (Eq. 17) combining the following three components
Sampler type	$u_{sampler}$	Random	Fixed values (8%[1] and 16%)
Laboratory analysis	u_{lab}	Random	Formula (Eq. 18, Gordon (2000))
Natural fluctuations of concentration	u_{nf}	Random	Repeated measures experiments (Sec. 2.2.9)
Systematic concentration errors	$u_{sys,C}$	Systematic	Formula (Eq. 15[1]) combining the four next components (3.54%)
Systematic lateral integration errors	$u_{sys,m}$	Systematic	Fixed value (1.5%[1])
Systematic vertical integration errors	$u_{sys,p}$	Systematic	Fixed value (2%[1])
Systematic laboratory analysis errors	$u_{sys,lab}$	Systematic	Fixed value (2%[1])
Systematic sampler type errors	$u_{sys,sampler}$	Systematic	Fixed value (1.5%[1])

[1] Value originating from ISO 4363 (2002)

where $u'_{\mathrm{sys,C}}$ is the uncertainty due to systematic errors in the concentration, u'_m is the uncertainty due to the lateral integration based on the number m of verticals and $u'_{p,l}$ is the total uncertainty due to the vertical integration estimated for each vertical l
265   (cf. Fig. 2).

2.2.3   Uncertainty due to systematic sources of error $u'_{\mathrm{sys,C}}$

Following the ISO 4363 (2002) method, the uncertainty due to systematic sources of error $u_{\mathrm{sys,C}}$ is expressed as:

$$u'^2_{\mathrm{sys,C}} = u'^2_{\mathrm{sys,m}} + u'^2_{\mathrm{sys,p}} + u'^2_{\mathrm{sys,lab}} + u'^2_{\mathrm{sys,sampler}}, \tag{15}$$

where $u'_{\mathrm{sys,m}}$ is the uncertainty due to the systematic error of the flux computation scheme, $u'_{\mathrm{sys,p}}$ is the uncertainty due to
270   the systematic error of the vertical integration, $u'_{\mathrm{sys,lab}}$ is the uncertainty due to the systematic error of the laboratory analysis and $u'_{\mathrm{sys,sampler}}$ is the uncertainty due to the systematic error of the sampler type, since the underlying errors are assumed systematic. These terms, detailed in ISO 4363 (2002), remain constant, independently of the increasing number of sampling points or verticals (cf. Table 1).

2.2.4   Uncertainty u'_m due to lateral integration

275   Ta facilitate the application compared to the standardized approach (ISO 4363, 2002), the uncertainty u'_m due to lateral integration, is estimated based on Eq. 3 and the nomograph published by Guy and Norman (1970):

$$u'_m = 0.4\, p_s\, (1.43\, \xi - 1.37)\, m^{-0.7}, \tag{16}$$

with p_s the percentage of sand in the suspension, ξ (cf. Eq. 3) the $\overline{v}^2/h$-index (Colby, 1964) and m the number of verticals. If only the suspended-sand flux through a cross section is measured or is of principal interest, as in our study, the percentage
280   of sand should be supposed to be 100 %, neglecting the fine-sediment flux. As a consequence, the uncertainty u'_m for the same sediment discharge measurement (same m and ξ) is higher, when assuming $p_s = 1$ than in sediment-flux measurements including fine sediments. This approach is applied in our study, although the lateral interpolation applied differs slightly, as it is based on the water depth h and the parameters C_R and α of the vertical profiles. However, this approach is assumed to be consistent with our modified lateral interpolation.

285   ### 2.2.5   Uncertainty u'_p due to vertical integration

The uncertainty u'_p is determined for each vertical l from the distribution of vertically integrated concentrations computed from the profiles estimated by the Bayesian approach described in Sec. 2.1.3. This uncertainty accounts for the uncertainty u'_{meas} (estimated in Sec. 2.2.6) in point concentrations taken as observational data in the Bayesian inference. The integration of the previously obtained vertical concentration profiles $\ln(C_n(z))$ (Sec. 2.1.3) allows the determination of the parametric
290   uncertainty $u'_{p,\mathrm{param}}$. However, computing the total uncertainty u'_p due to vertical integration requires the inclusion of structural errors at the elevation of the sampling points prior to the vertical integration. These structural errors are representative of the

residuals between the point measurements and the exponential profiles. The structural uncertainty can be estimated from the total uncertainty u'_p and the parametric uncertainty $u'_{p,\mathrm{param}}$: $u'_{p,\mathrm{struc}}$ as $u'^2_{p,\mathrm{struc}} = u'^2_p - u'^2_{p,\mathrm{param}}$.

295 The parametric uncertainty $u'_{p,\mathrm{param}}$ can be determined from the distribution of concentration profiles $\ln(C_n(z))$ computed in Sec. 2.1.3 (Fig. 3a). Each of these n profiles is converted to $C_n(z)$ (Fig. 3b) and linearly interpolated applying a trapezoidal integration to determine its depth-averaged concentration $\overline{C_n}$, which is converted to $\ln(\overline{C_n})$. Application of the entire procedure for all simulations n, then yields a distribution of depth-averaged concentrations $\ln(\overline{C_n})$. The mean value of this distribution is $\overline{\ln(\overline{C})}$ and the standard deviation is the uncertainty $u'_{p,\mathrm{param}}$ based on the assumption $\sigma = u'_{p,\mathrm{param}}$ (Fig. 3c).

To determine the structural error, the prior distribution of its standard deviation is defined as log-normally distributed with
300 $\mu = 0$ and $\sigma = 1$ in the BaM! method. For every sampling point at the elevation z, a normally distributed error with mean zero and standard deviation u'_{meas} is defined. An error is then drawn from this distribution and added to the estimated concentration $\ln(C_n(z))$ for every simulation n to obtain a modified vertical profile $\ln(C_{\mathrm{mod,n}}(z))$ (Fig. 3d). In the next step, the same procedure as for the estimation of $u'_{p,\mathrm{param}}$ is applied: conversion of $\ln(C_{\mathrm{mod,n}}(z))$ to $C_{\mathrm{mod,n}}(z)$, vertical averaging to obtain $\overline{C_{\mathrm{mod,n}}}$ and conversion to $\ln(\overline{C_{\mathrm{mod,n}}})$. The mean value of the resulting distribution is the mean depth-averaged concentration
305 $\overline{\ln(\overline{C_{\mathrm{mod}}})}$ and its standard deviation is the total uncertainty u'_p due to vertical integration, based on the assumption $\sigma = u'_p$ (Fig. 3f).

2.2.6 Uncertainty u'_{meas} in point concentrations

As point concentration errors are accounted for in the Bayesian analysis of vertical concentration profiles, the uncertainty u'_{meas} in point concentrations is already included in the uncertainty u'_p due to vertical integration. Therefore, in contrast to the ISO
310 4363 (2002) method, u'meas does not explicitly appears in Eq. 14. The uncertainty u'_{meas} is calculated as:

$$u'_{\mathrm{meas}} = \sqrt{u'^2_{\mathrm{sampler}} + u'^2_{\mathrm{lab}} + u'^2_{\mathrm{nf}}}, \tag{17}$$

where u'_{sampler} is the uncertainty due to the sampler type, u'_{lab} is the uncertainty due to the laboratory analysis and u'_{nf} is the uncertainty due to natural fluctuations in sediment concentration arising from turbulence (Fig. 2).

2.2.7 Uncertainty u'_{sampler} due to the sampler type

315 Even though several comparisons have been conducted, the distribution of random errors related to a specific sampler type is difficult to assess. For example, a review of the values of u'_{sampler} used in different studies is provided by Dramais (2020). In this study, the value suggested in the ISO 4363 (2002) standard is used for isokinetic samplers such as the US P6: $u'_{\mathrm{sampler}} = 8\ \%$. To account for the greater uncertainty arising from non-isokinetic sampling, this uncertainty is arbitrarily doubled for non-isokinetic samplers: $u'_{\mathrm{sampler}} = 16\ \%$.

320 ### 2.2.8 Uncertainty u'_{lab} due to laboratory analysis

Many studies have estimated the random uncertainty related to the measurement of (fine) sediment concentration in the laboratory (e.g. by filtration). The ISO method estimates an uncertainty of 1.5 % due to the random error and an uncertainty of 2 %
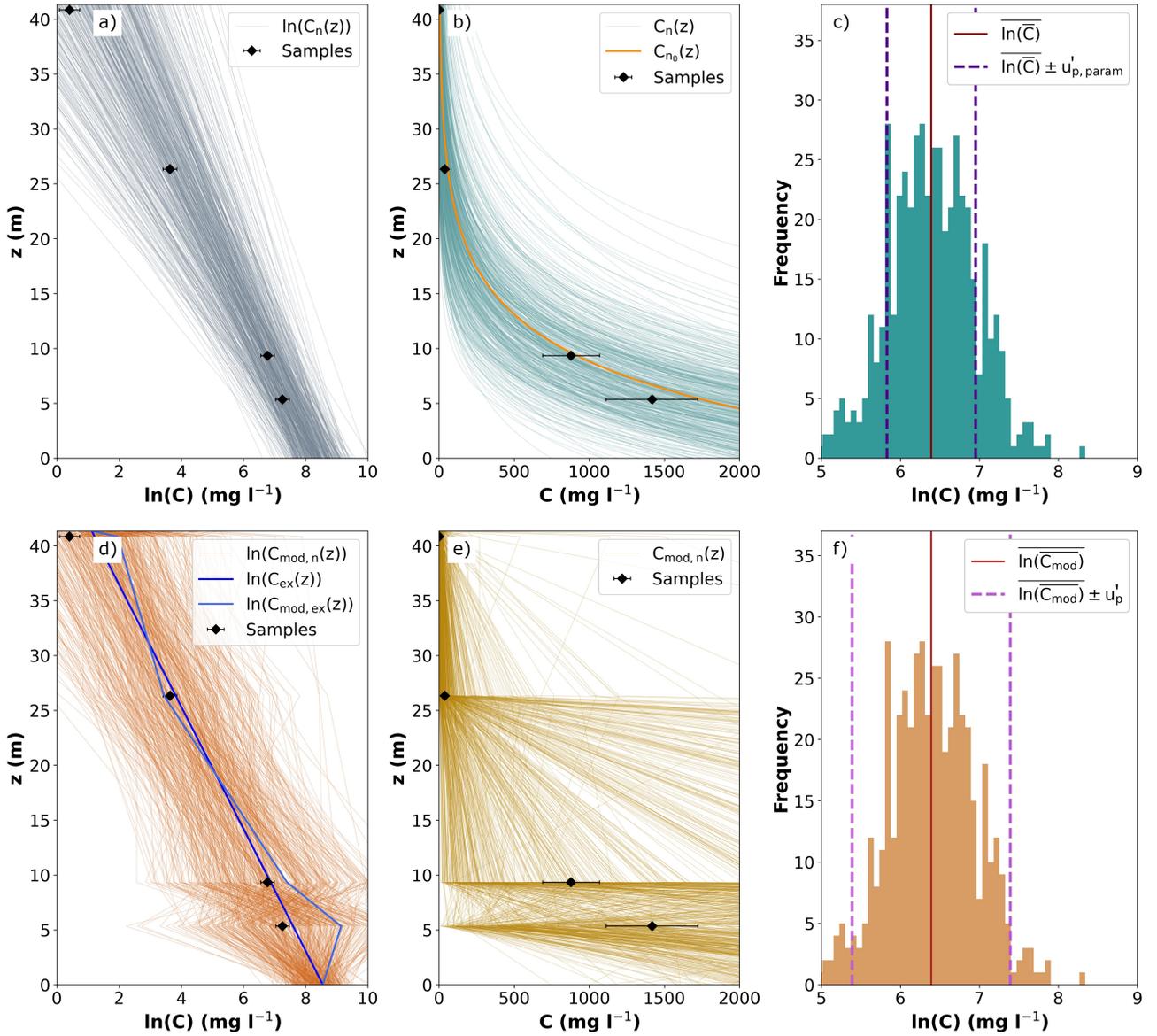
Figure 3. Workflow for the estimation of the uncertainty u'_p due to vertical integration, including the estimation of the parametric uncertainty $u'_{p,\mathrm{param}}$ in a,b,c) and of the total uncertainty u'_p in d,e,f). a,d) Vertical concentration profiles $\ln(C_n(z))$ and $\ln(C_{\mathrm{mod,n}}(z))$, respectively, sampled through Bayesian interference and including the structural error and two exemplary profiles in d). b,e) Vertical concentration profiles $C_n(z) = \exp(\ln(C_n(z)))$ and $C_{\mathrm{mod,n}}(z) = \exp(\ln(C_{\mathrm{mod,n}}(z)))$, respectively, with the MaxPost profile $C_{n_0}(z)$ in b). c,f) Histograms of depth-averaged concentrations $\ln(\overline{C_n})$ and $\ln(\overline{C_{\mathrm{mod,n}}})$ with the mean depth-averaged concentrations $\overline{\ln(\overline{C})}$ and $\overline{\ln(\overline{C_{\mathrm{mod}}})}$ as well as the standard deviations $u'_{p,\mathrm{param}}$ and u'_p, respectively.

due to the systematic error (ISO 4363, 2002). Based on an intercomparison study of different laboratories, Gordon et al. (2000) determined a standard uncertainty for the fine and sand fractions separately. We use the approach of Gordon et al. (2000) at the

325 68 % confidence level and a given sand concentration C (g l^{-1}) in the analysed sample:

$$u'_{\mathrm{lab}} = 1.091\,C^{-0.5}. \tag{18}$$

2.2.9 Uncertainty u'_{nf} due to natural fluctuations

To approximate the uncertainty u'_{nf} due to the natural fluctuations in concentration and grain size in the point samples arising from turbulence, a simplified method, similar to the ISO method or the "At-a-Point-Error" (APE) Topping et al. (2011) is

330 applied. To this end, several points are repeated at different hydro-sedimentary conditions with a time difference of less than 1 hour between the first and last sample and the suspended-sand concentration C_i is calculated for each sample. One sampling point is repeated three to nine times and the mean sediment concentration $\overline{C_{\mathrm{rep}}}$ of the respective set of measurements is determined. Based on the nomenclature of the ISO 4363 (2002), this mean concentration $\overline{C_{\mathrm{rep}}}$ per set can be understood as the "approximate true value". The relative standard deviation u'_{rep} for each set of n_{rep} repetitions is then calculated following ISO

335 4363 (2002):

$$u'_{\mathrm{rep}} = \sqrt{\frac{\sum_{i=1}^{n_{\mathrm{rep}}} \left(\frac{C_i}{\overline{C_{\mathrm{rep}}}} - 1 \right)^2}{n_{\mathrm{rep}} - 1}} \tag{19}$$

Performing this calculation for all repetitions, the relative uncertainty for each set of repetitions u'_{rep} can be plotted versus the mean concentration $\overline{C_{\mathrm{rep}}}$ per set (Fig. 4).

The number of sets of repetitions and tested hydro-sedimentary conditions within this study is limited compared to the variety

340 of sampling conditions. In the best case, these measurements should be conducted on every sampling campaign, however, in reality, this is not possible. The sampling campaign with additional samples for the uncertainty estimation would take very long, so that the variation in river discharge would become too great. Therefore, a constant uncertainty $u'_{\mathrm{nf}} = 14.24$ % is determined based on these results and applied to all point measurements, which corresponds to the median of all tested relative uncertainty u'_{rep}. The enlarged uncertainty of $U'_{\mathrm{nf}} = 28.47$ % at a 95 % confidence interval corresponds roughly to the estimations made

345 by Gitto et al. (2017) in the Canadian Fraser River (they found 3 to 33 % of uncertainty range for individual 30 s samples). Furthermore, it should be noted that only a small range of hydro-sedimentary conditions at a given sampling location is sampled by this empirical approach. The uncertainties are probably higher than estimated here and may as well be grain-size dependent (Topping et al., 2011).
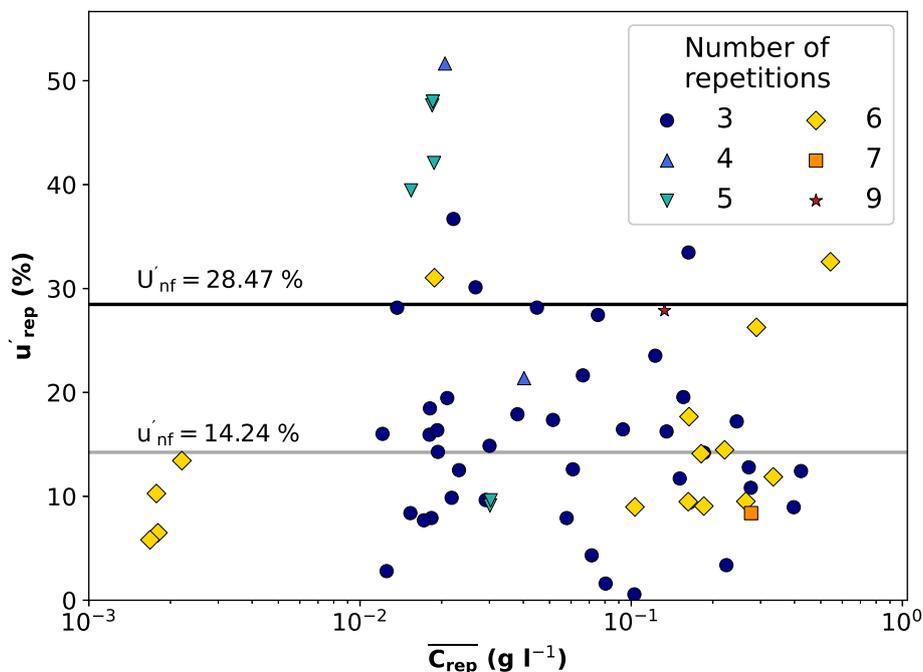
Figure 4. The relative uncertainty u'_{rep} and mean concentration $\overline{C_{\mathrm{rep}}}$ for each set of repetitions (these repetitions include data from Isère, Colorado, Toutle, and Cowlitz Rivers (Spicer, 2019)).

3 Application

3.1 Survey sites

The proposed SDC method was applied to four datasets from different rivers around the world. Each dataset includes suspended-sediment measurements following the above presented protocol and ADCP data.

3.1.1 Rhône River

The Rhône River is one of the major rivers of Europe, heading from the Rhône Glacier in the Alps, and running through western Switzerland and south-eastern France. Mostly a gravel-bed river, it is the largest silt and clay contributor to the Mediterranean sea (Delile et al., 2020). The presented measurements were conducted near the gaging station (V3000015) at Lyon Perrache (WGS84 coordinates: 45.742344, 4.826738), France, where the Rhône River drains a catchment of about $20\,300$ km^2 with a mean annual discharge of about 600 m^3 s^{-1} (Dramais, 2020).

3.1.2 Isère River

360 The Isère River is an Alpine river and the largest tributary of the Rhône River by suspended sediment flux (Poulier et al., 2019). At Grenoble, France (WGS84 coordinates: 45.197747, 5.768566) , where the measurements were conducted (gaging station W1410010) (Némery et al., 2013), the mean annual discharge is about 180 m^3 s^{-1} with a catchment area of 5 700 km^2.

3.1.3 Colorado River

The Colorado River is one of the most iconic rivers in the western USA. The measurements took place at the U.S. Geological
365 Survey (USGS) Colorado River above Little Colorado River near Desert View (WGS84 coordinates: 36.203484, -111.800917), Arizona gaging station at the River Mile 61. This station (number 09383100) has a mean annual discharge of 306 m^3 s^{-1} and a catchment area of 296,000 km^2. Suspended-sediments are monitored since a long time in this area (Grams et al., 2015).

3.1.4 Amazon River

The Amazon River basin exceeds 6 000 000 km^2 in area. The Amazon River is the largest river in the world by discharge. The
370 Manacapuru gauging station (14100000) is part of the Critical Zone Observatory HyBAm (Hydrology of the Amazon Basin) and operated by the French National Research Institute for Sustainable Development (IRD), the Brazilian National Agency (ANA), and the Brazilian Geological Service (CPRM). This station has been used for more than 40 years by the Brazilian national hydrometric network to provide data on the Amazon (Solimões) River (WGS84 coordinates: -3.324377, -60.561183). At this station, the Amazon River watershed is approximately 2×10^6 km^2 and average water discharge is about 103 000 m^3 s^{-1}
375 (Filizola et al., 2009).

Those four survey sites, with various geomorphological conditions (see Table 2), were sampled according to the above-described ADCP-measurement and point-sampling procedures. The Isère River was sampled with an isokinetic US P-06 sampler and the other rivers with watertrap-type sampler (Niskin).

380 3.2 Vertical suspended-sand concentration and flux profiles

Measured suspended-sand point concentrations are fitted with an exponential profile to extrapolate the concentrations to the unmeasured parts of the water column and also interpolate between points. There is substantial vertical and lateral variability in suspended-sand concentration at all study sites (Fig. 5). Indeed, different vertical gradients α and/or reference concentrations C_R are observed among the measured verticals. The highest sand concentrations and largest gradients, with a difference of up
385 to three orders of magnitude between the bottom and surface concentrations, are observed in the Amazon River (cf. Fig. 5d). In contrast, the concentrations at the other sites range between 0.01 and 0.5 g l^{-1}. In the various surveys, sand-concentration gradients are associated with particle-size gradients, with coarser particles closer to the riverbed. The measured concentrations vary strongly at some verticals, so that they do often not correspond to the fitted vertical concentration profiles, not even when

Table 2. Hydraulic and morphological characteristics of the survey sites. Q_w is the total ADCP water discharge including extrapolations areas, $Q_{\mathrm{Meas.}}$ is the ADCP measured water discharge (excluding extrapolations areas), $\bar{v}$ the mean cross-sectional velocity, the aspect ratio is the river width divided by mean depth, D_{50} is the median diameter of suspended-sand, p_s the percentage of sand in the suspension, ξ is an index relating stream velocity and depth, and U'_Φ is the expanded uncertainty in measurements of suspended sand flux at 95% confidence level.

River and location	Survey date	Q_w (m³ s⁻¹)	$Q_{\mathrm{Meas.}}/Q_w$ (%)	$\bar{v}$ (m s⁻¹)	W (m)	H (m)	Aspect ratio (-)	Sand D_{50} (μm)	p_s (%)	ξ (-)	U'_Φ (%)
Rhône at Lyon Perrache (France)	Jan. 22th 2018	2000	81	1.2	170	12	14	100-300	26.9	1.07	18.6
Isère at Grenoble (France)	Apr. 6th 2022	120	52	1.1	70	3	23	90-290	46.6	1.23	19.1
Colorado River Mile 61 (USA)	Feb. 19th 2019	370	65	1.1	100	5	20	100-130	68.2	1.6	31.1
Amazon at Manacapuru (Brazil)	Apr. 19th 2012	144000	83	1.6	3400	43	79	180	76.6	1.33	26.6

taking the uncertainty U'_{meas} on the point concentrations into account. This uncertainty usually varies for the presented samples
390 between 20 and 25 % at a 95 % confidence interval.
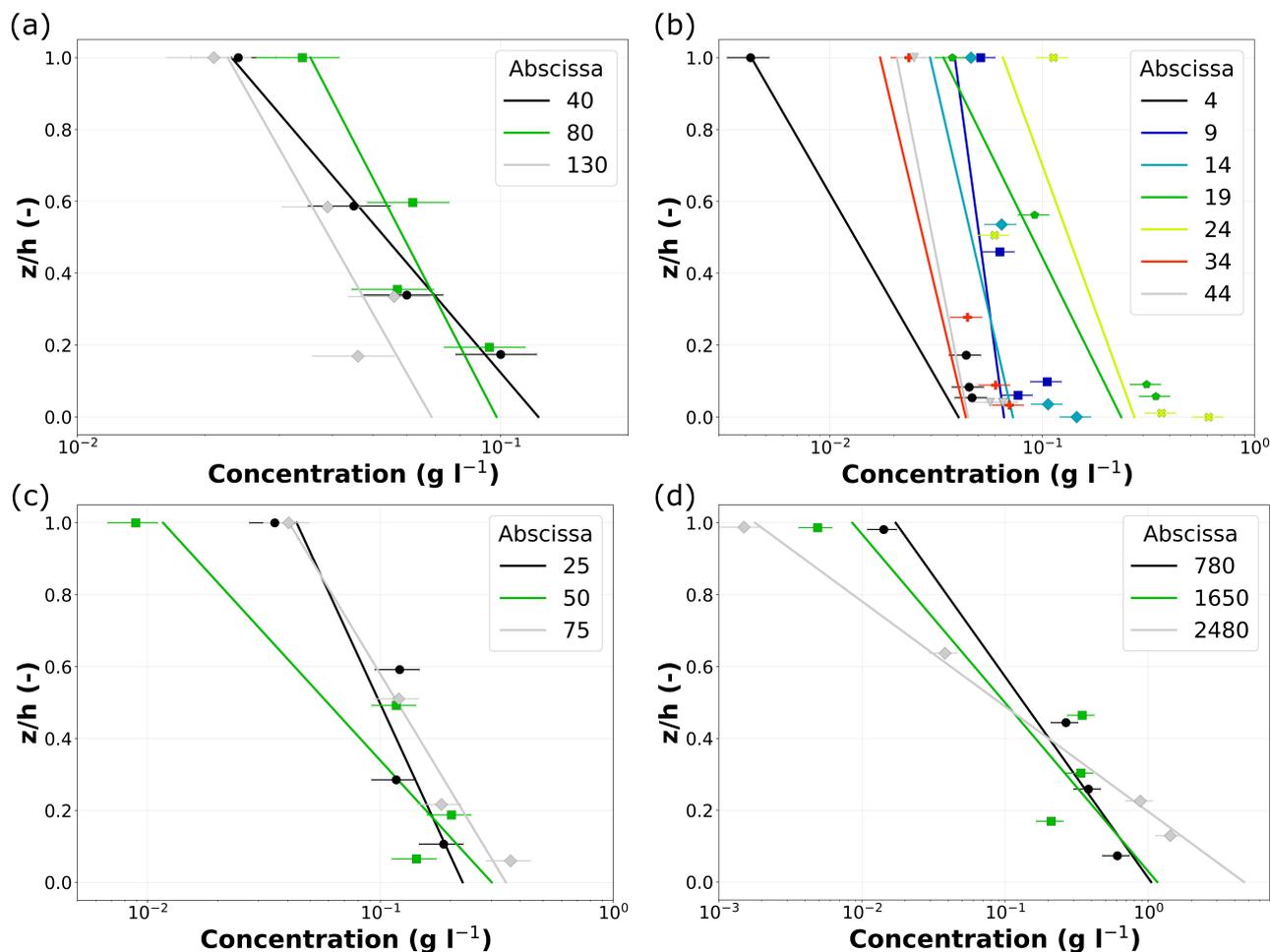
Figure 5. Measured sand concentrations with uncertainty U'_{meas} and exponential fits using Bayesian modelling for the Rhône River at Lyon Perrache (a) Isère at Grenoble Campus (b), Colorado River at River Mile 61 (c) and Amazon River at Manacapuru (d).

Vertical profiles of suspended-sand flux (Fig. 6) are determined by multiplying the suspended-sand concentration in each cell in the MAP-grid with the discharge in the same cell. Similarly, the point suspended-sand fluxes are the product of the point concentration and the discharge of the surrounding cell in the MAP-grid. Consequently, decreasing fluxes close to the bed, as expected based on theory, are hardly or not at all visible for most verticals sampled in the Isère (Fig. 6b) or the Colorado

395 (Fig. 6c). Large differences between the point fluxes and the profiles result notably from poorly fitted vertical concentration profiles, e.g. vertical 34 in the Isère River or vertical 1650 in the Amazon River. In other words, when the point concentrations do not follow an exponential profile, there are large differences between point fluxes and profiles.
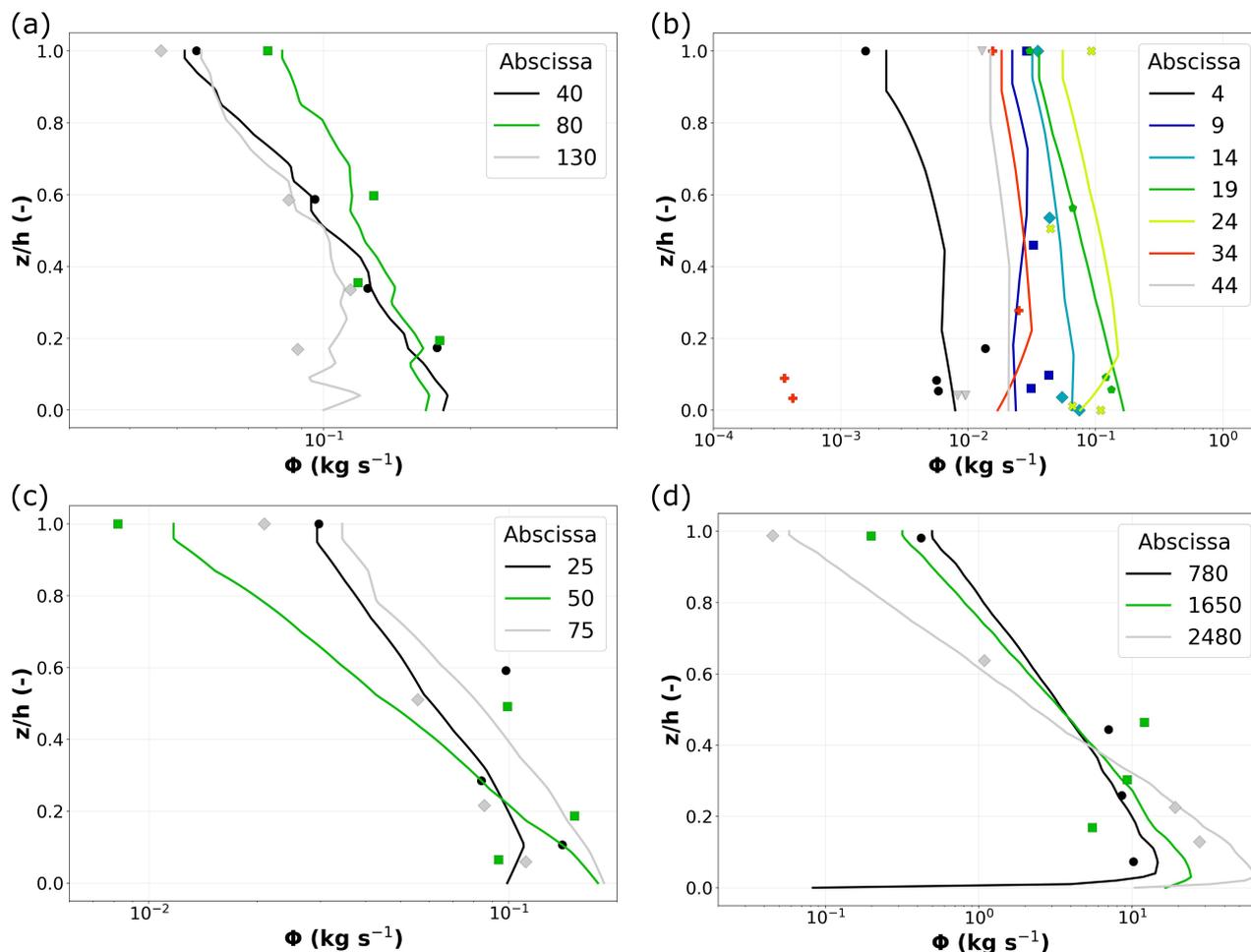
Figure 6. Suspended-sand fluxes in the sampling verticals and at the sampling points for the Rhône River at Lyon Perrache (a) Isère at Grenoble (b), Colorado River at River Mile 61 (c) and Amazon River at Manacapuru (d).

3.3 Suspended-sand flux through a cross section

The suspended-sand concentration in each MAP cell (i, j) is calculated by applying the lateral interpolation and extrapolation of the profile coefficients C_R and α (Sec. 2.1.3). The spatial view of the cross sections highlights the distribution of the suspended-sand concentration (Fig. 7). Different layers in some measurements appear due to the vertical and horizontal resolution of the ADCP data, i.e. the size of the MAP cells. As the vertical integration is based on the water depth, the lateral interpolation of the profile coefficients produces high concentrations near the bed, especially when there are large water depth variations and when vertical measurements are made on the deepest parts. This is clearly observed Fig. 7d in between the central and right sampling vertical on the Amazon.
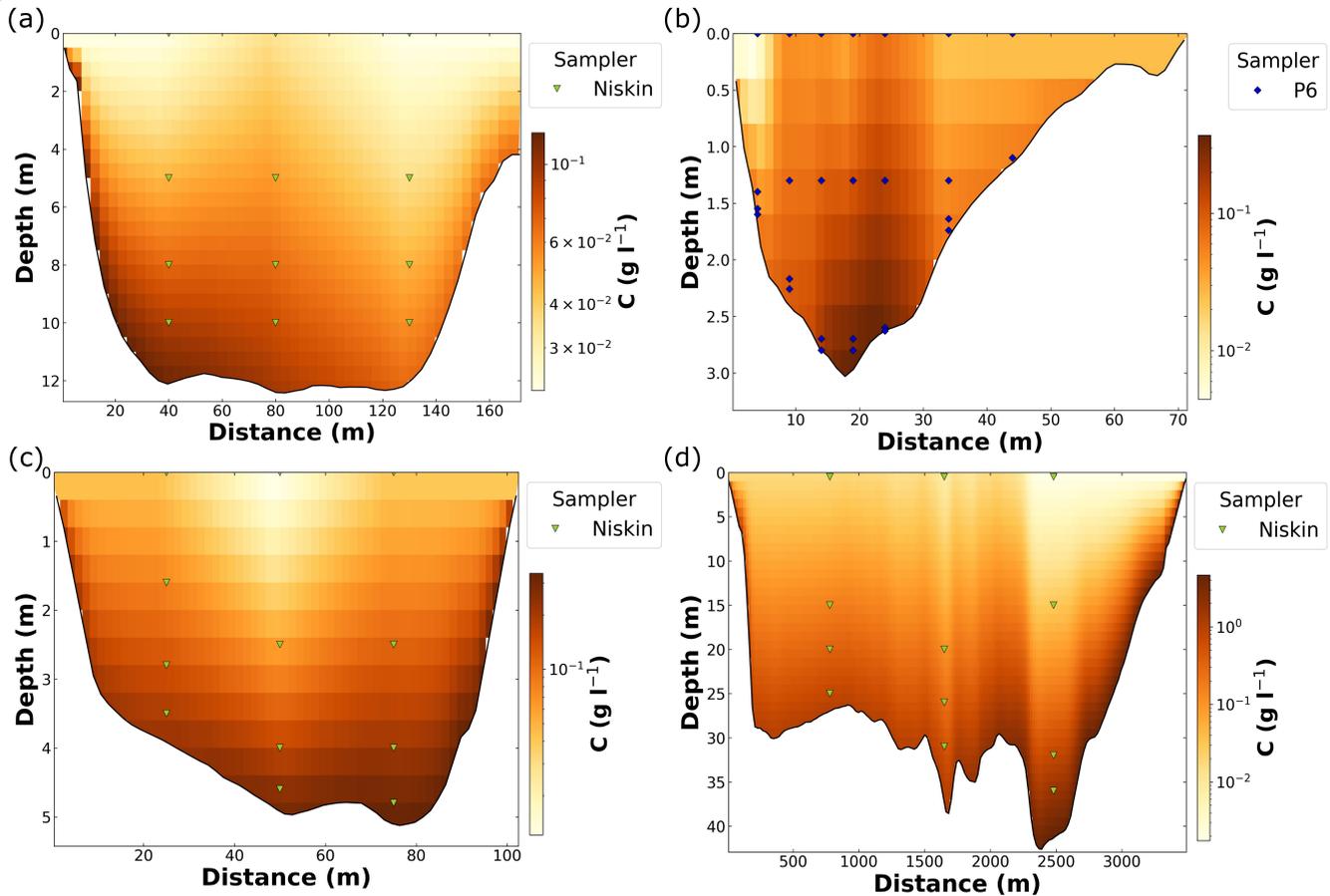
Figure 7. Suspended-sand concentrations calculated with SDC method throughout the cross section of the Rhône River at Lyon Perrache (a), the Isère River at Grenoble Campus (b), the Colorado at River Mile 61 (c) and the Amazon River at Manacapuru (d).

The mean cross-sectional suspended-sand concentrations $\overline{C_{\mathrm{SDC}}}$ and fluxes Φ_{SDC} computed with the SDC method, are compared to the ISO method (ISO 4363, 2002) are compared using the relative differences $\epsilon_C = (C_{\mathrm{SDC}} - C_{\mathrm{ISO}})/C_{\mathrm{ISO}}$ and ϵ_Φ, respectively. The results for the suspended sand concentration are in close agreement between the two methods, with ϵ_C ranging between -2 and 3.5 % for three examples (Table 3), whereas a significant concentration difference is observed between both methods for the Colorado computations (-15.8 %). The most likely hypothesis to explain this difference is that the surface sample at the middle of the transect has a relatively low sand concentration (abscissa 50, Fig. 5c). This low concentration heavily leveraged the fit of the vertical profile and reduced the flux in this part of the cross section, which is the place of the most intense flow. This highlights one of the limitations of the method when only a few points are used for suspended-sand flux computation in the cross section.

Table 3. Mean cross-sectional suspended-sand concentrations and total fluxes for the four presented measurements using the ISO method and SDC method.

Study site	$\overline{C_{\mathrm{ISO}}}$ (g l^{-1})	$\overline{C_{\mathrm{SDC}}}$ (g l^{-1})	ϵ_C (%)	Φ_{ISO} (kg s^{-1})	Φ_{SDC} (kg s^{-1})	ϵ_Φ (%)
Rhône River	0.051	0.050	-2.0	102	99.3	-2.8
Isère River	0.085	0.088	3.5	9.2	9.5	2.9
Colorado River	0.120	0.101	-15.8	48.1	40.5	-16
Amazon River	0.304	0.298	-2.0	40284	39438	-2.1

3.4 Suspended-sand uncertainty evaluation

The total uncertainty and the contribution of each error source to total variance are evaluated for the four measurements (Fig. 8). The absolute uncertainty at a 95 % confidence interval with a coverage factor of $k = 2$ ranges between 19 % and 31 %. The main uncertainty components are the uncertainty U'_p due to vertical integration and the uncertainty U'_m due to lateral integration. The uncertainty U'_p is displayed as its two components, the parametric uncertainty $u'_{p,\mathrm{param}}$ and the structural uncertainty $u'_{p,\mathrm{struc}}$. The parametric uncertainty $u'_{p,\mathrm{param}}$ is determined by the information from the priors and from the sampling points used to calibrate the model, particularly their number, distribution along the vertical, and uncertainty u'_{meas}. Increasing the number of samples and decreasing the uncertainty u'_{meas} would decrease this uncertainty $u'_{p,\mathrm{param}}$. In contrast, the structural uncertainty $u'_{p,\mathrm{struc}}$ is estimated from the residuals of the fit of the model to the calibration points. The farther they are from the fitted vertical concentration profile and the lower their uncertainty, the greater is the uncertainty $u'_{p,\mathrm{struc}}$.

The uncertainty U'_m is estimated from index ξ, representing the lateral homogeneity of the cross section in terms of depth and discharge with the percentage of sand in the suspension and the number of sampling verticals. However, as only sand concentrations are considered here, the percentage of sand was set equal to 100 %. At relatively high ξ-values, such as on the Colorado River, a larger number of verticals would have been required to decrease the uncertainty U'_m, whereas this uncertainty is relatively low in a more uniform river like the Rhône River with a low ξ-value. In that latter case, three verticals are sufficient to describe the lateral distribution of the concentration in the cross section. The measurements on the Isère and Amazon Rivers are both characterized by similar ξ. The large number of sampling verticals in the Isère River (seven) leads to a low uncertainty U'_m, whereas the uncertainty and small number of sampling verticals in the Amazon River (three) leads to high uncertainty U'_m. Nevertheless, it has to be taken into account that the lateral integration is based on the water depth, whereas the calculation of the uncertainty U'_m is based on ξ. These two different ways to conduct the lateral integration of the suspended-sand concentration and the uncertainty estimation may affect the results. The contributions of both the uncertainties U'_Q on the liquid discharge and the systematic uncertainties u'_{sys} to the uncertainty U'_Φ on the suspended-sand flux are typically low.
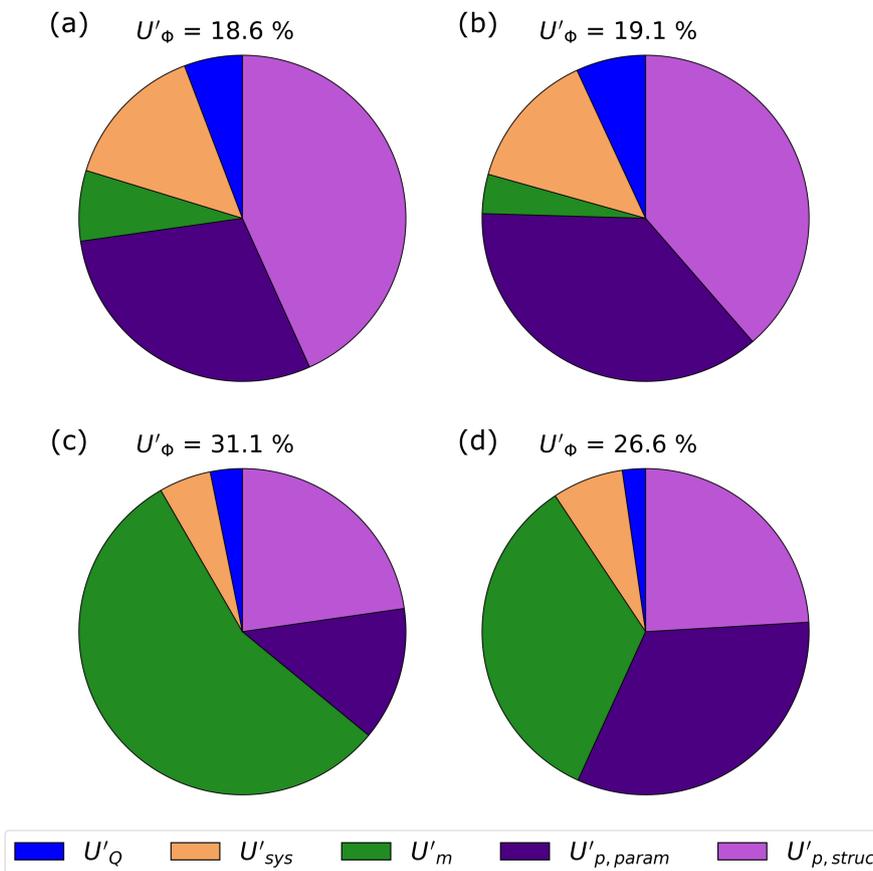
Figure 8. Total flux uncertainty U'_Φ and the relative contributions of uncertainty components to the total variance on the Rhône River at Lyon Perrache: (a), on the Isère River at Grenoble (b), on the Colorado at River Mile 61 (c) and on the Amazon River at Manacapuru (d).

4 Discussion

4.1 A physically based method

440   The novel SDC method offers a number of advances for cross-sectional sediment flux measurement, especially the physically based integration of concentration.

    For the vertical integration of concentration, the first step of the method is based on the fit of an exponential profile. The uncertainty related to the fit of this profile is estimated. As discussed in Camenen and Larson (2007), very similar results would have been obtained by fitting a Rouse profile. However, another more detailed approach (Hunt, 1969; McLean, 1992)
445   may provide a better fit and thus modify the results. Consequently, various theoretical approaches including the effects of stratification by suspended-sediment or due to size distribution of sediment may be integrated into the toolbox, allowing to

choose the best fitting semi-empirical model to the sampling conditions. Until now, only the exponential profile and the Rouse profile (not presented here, but included in the code) are available in the toolbox.

The goodness of the fit, thus the structural uncertainty, depends not only on the chosen profile, but also on the number and position of the sampling points. Dramais (2020) applied the same Bayesian approach and showed that the points measured close to the bed have a great influence on the reference concentration C_R value and on the slope α of the fitted exponential profile. In contrast, subsurface samples may in some cases bias the fit of the exponential profile. Interestingly, the best compromise was observed when sampling points are positioned close to the bed and for a number of five samples per profile.

Depth-integrating measurements could be a solution to avoid errors due to the vertical interpolation which occur with fitting point samples. However with this protocol, lateral extrapolations and extrapolations in the unmeasured parts of the cross-section are not possible with a physical base. Depth-integrating samples could then be associated with a larger uncertainty.

The lateral integration of the concentration may be improved as well, even though the SDC method presents an advance by using the water depth as a proxy for the shear stress. The current method leads to artefacts of relatively high concentrations close to the river bed within extrapolated areas (Fig. 7d).

A major advance in both the vertical, but particularly the lateral integration, may be made using the acoustic backscatter measured by the ADCP. The backscattered signal intensity maybe used as a proxy for suspended-sediment concentration and grain size. Several studies (Bouchez et al., 2011; Venditti et al., 2016; Szupiany et al., 2019) and commercial softwares (e.g. ASET (Dominguez Ruben et al., 2020)) focus on the vertical moving-boat backscatter inversion to gain information on suspended-sediment. Nevertheless, for single-frequency applications as the ADCP, strong assumptions or calibrations are necessary to estimate correctly the concentration and grain size of silt-clay and sand-sized sediment (Vergne et al., 2023). Additionally, the issue of unmeasured areas close to the river bed, surface and banks persists and requires the extrapolation of the estimated concentrations, e.g. by applying theoretical suspended sand transport formulas (Dominguez Ruben et al., 2020).

4.2 A high-resolution ADCP data based method

Our study proposes a general method which uses high-resolution ADCP data from successive transects. Compared to existing multi-transect averaging tools, the newly developed ADCP multi-transect averaged profile (MAP) provides a complete single-transect average dataset including the unmeasured areas. MAP uses RDI or SonTek raw binary files, and reduces the pre-processing error, as it uses data quality filters from QRevint. The method may use either the bottom track or the GPS as reference and the user can customize vertical and lateral dimensions of the resulting grid cells. The obtained regular grid then facilitates the further analysis steps.

One limitation of the SDC method is due to the vertical and lateral integration of concentrations which can be limited by the ADCP data resolution. The vertical and lateral integration of concentration are evaluated on each MAP grid cell. Although this approach allows the estimation of concentrations close to the bed and banks, the size of the grid cells is limited by the size of the ADCP cells. Consequently, if the ADCP spatial resolution is low and the resulting mean concentration may be affected. An example of this problem is provided by the data from the Colorado River (Fig. 9), where cells were set with a height of approximately 0.4 m (Fig. 9a) and 0.8 m (Fig. 9b). In some cases, it could be meaningful to adapt the ADCP cells

size to increase the resolution of the measurement and consequently increase the resolution of the resulting cross-sectionnal estimation of the distribution of the sediment flux.
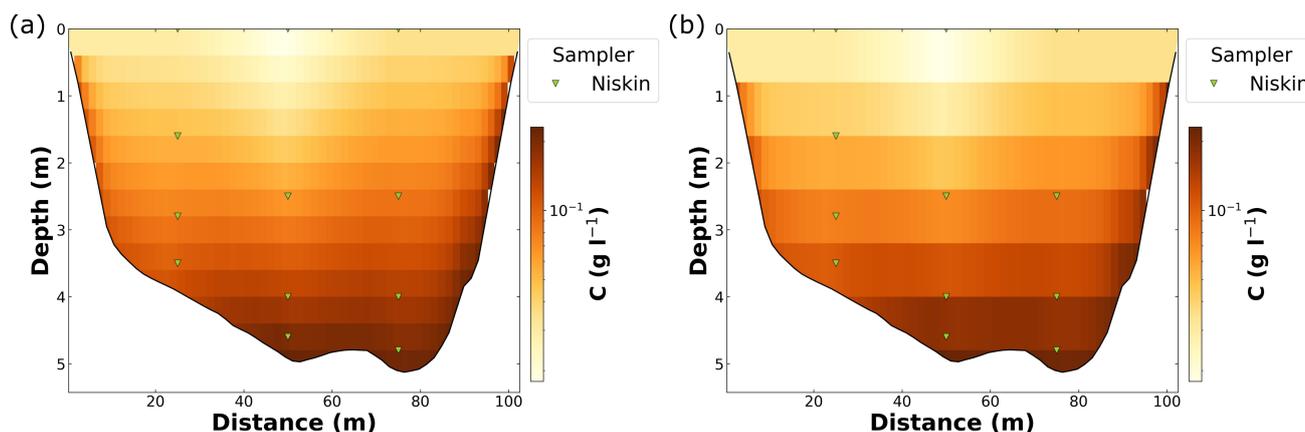
Figure 9. Influence of the vertical cell height on the cross-sectional suspended-sediment measurement in the Colorado River at River Mile 61, a) with a cell height of 0.4 m and b) with a cell height of 0.8 m.

4.3 A method open to various sampling protocols

Another advantage of the SDC method is its suitability to different point sampling protocols, with various numbers and lo-
485 cations of sampling points along the verticals and varying numbers of verticals. This flexibility is particularly useful, when specific areas or depths are of major interest requiring more detailed sampling or if the sampling points are not distributed in the cross section following the ISO protocols. Also, it provides an estimation of the suspended-sand concentration close to the bed or banks, in areas excluded by many methods such as the ISO method.

We evaluate the differences of the suspended-sand flux calculated using the proposed SDC method relative to the flux
490 calculated using the ISO method using a larger dataset for Rhône River and Isère River that encompasses the detailed examples shown above. For this supplementary data, conditions were different but they were at the same locations. The relative difference ϵ_Φ ranges for all four studied rivers between -15.9 % and +2.9 % with no clear relationship with the total flux (Fig. 10). In comparison, typical ADCP water discharge measurements are characterized by an uncertainty of 5 - 12 % (results from several repeated measures experiments performed in France (Despax et al., 2019)).

495 The sand fluxes results from the SDC method can differ from the results from the ISO method up to 15% even though they are calculated using the same measurement data. Some differences are observed, the main reason for these differences may be that the ISO method is based on a sampling protocol with seven points per vertical, where the samples are taken at precise relative depths. This recommended protocol is not followed in the presented measurements, typically, four samples are taken per vertical and at varying relative depths not corresponding to the ISO method. Notably during high discharges or for deep
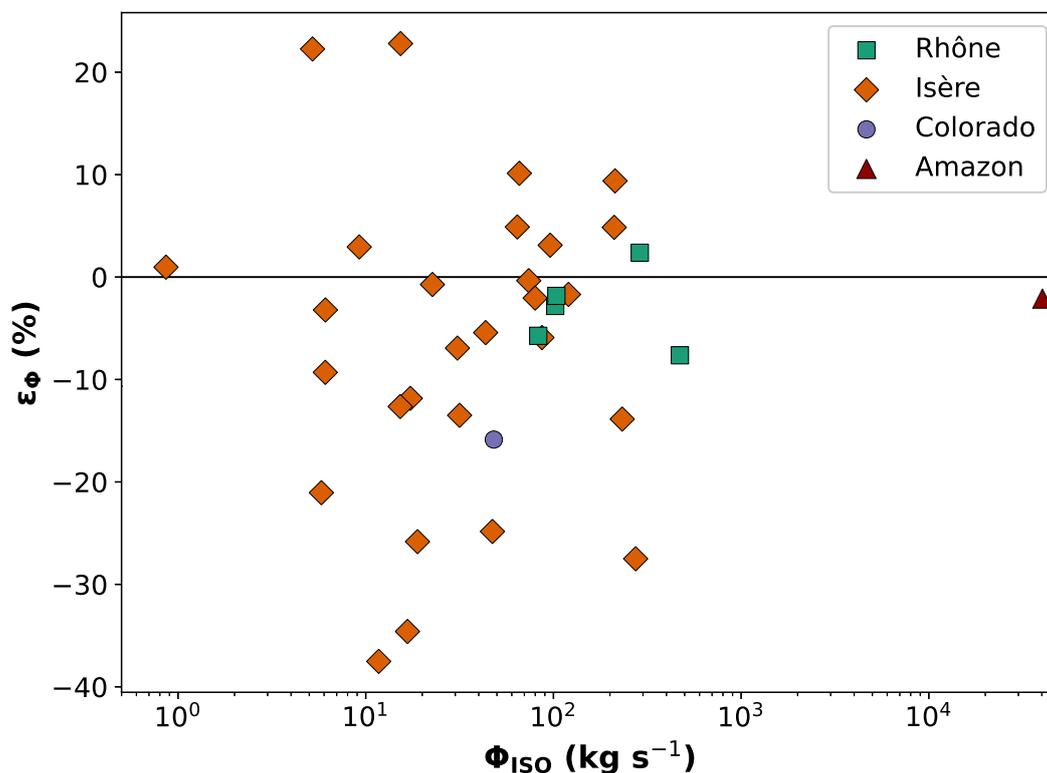
Figure 10. Relative difference $\epsilon_\Phi = (\Phi_{\mathrm{SDC}} - \Phi_{\mathrm{ISO}})/\Phi_{\mathrm{ISO}}$ as a function of the suspended-sand flux Φ_{ISO} determined using the ISO method for all four studied rivers, Φ_{SDC} is determined using the SDC method for all four studied rivers.

500   water depths, when it is difficult to lower the sampler close to the river bed, the SDC method may be be more accurate than the ISO method. However, accurate flux references are lacking in rivers, so that this assumption cannot be verified experimentally.

4.4   A first estimation of the suspended-sand flux uncertainty

This method combines existing and novel approaches to estimate the uncertainty in the suspended-sand flux taking all error sources into account and their contributions in the uncertainty budget, which represents a major advance over the existing ISO

505   method. The method is easy and fast to apply and contains no empirical calculation, except for the uncertainty u'_{nf} on natural concentration fluctuations. Compared to the ISO method, this reduces considerably the required sampling time and effort. Our method allows to interpolate and extrapolate concentrations based on a physically based approach. Furthermore, the introduced Bayesian approach we introduced to compute u'_{p} appears to be a promising way to analyze vertical concentration profiles and the related uncertainties.

510   This new approach does not have only advantages, and certain limitations have already been identified. Here are some suggestions for correcting them or improving the code. Concerning the uncertainty estimation, major advances could be made

by developing a more robust method for the estimation of the uncertainty u'_m due to the lateral integration, the uncertainty u'_{sampler} due to the sampler and the uncertainty u'_{nf} due to the natural fluctuations. The major issue about the estimation of the uncertainty u'_m is its difference to the physical approach followed for the lateral integration of the concentration. The

515   determination of the $\overline{v}^2/h$-index, ξ, accounts for the water depth and the stream velocity, whereas only the water depth is taken into account for the lateral interpolation of the concentration. Developing a consistent method for both uses and adapted to various channel geometries and lateral concentration gradients is needed. Similarly, robust methods to estimate the uncertainty u'_{sampler} due to the sampler and the uncertainty u'_{nf} due to natural fluctuations for different settings should be developed. Finally, potentially uncovered error sources such as the uncertainty in the vertical position and the uncertainty related to the

520   total sampling duration (Topping et al., 2011; Gitto et al., 2017) should be estimated and integrated as well. Moreover, the estimation of the prior distributions of α and $\ln(C_R)$ to estimate the uncertainty u'_p due to the vertical integration could be estimated as well.

4.5   An open source method

A fully operational and open-source toolbox is available. This toolbox includes several options not presented in this article. The

525   code is relatively flexible, suitable for various conditions and protocols commonly applied in point sampling protocols. It allows the computation of suspended-sand, but also silt-clay concentration if available for various sampler types and deployment conditions. If silt-clay concentrations are available, the ratio of silt-clay concentration to sand concentration can be compared at each sampling point and also over the entire cross section. The vertical position of the sampler may be determined as well as the transit time between the water surface and the final sampling depth if pressure-sensor measurements are available.

530   If available, the results of the flux measurements may be related to data from adjacent hydro-sedimentary gauging stations. If grain-size data are available for several samples, they are visualized and a mean cross sectional grain size distribution following ISO 4363 (2002) is calculated.

5   Conclusion

The new SDC method presented in this study allows meaningful determination of the suspended-sand flux through a river

535   cross section with uncertainty. Therefore, this method merges data from ADCP discharge measurements and point suspended-sediment samples. The SDC method includes a method for averaging several ADCP transects with discharge and velocity measurements on a regular grid in the entire cross section is developed. Suspended-sand concentrations obtained by point sampling are then vertically interpolated by fitting a physical-based exponential concentration profile and choosing the best fit using a Bayesian framework (BaM!). The lateral interpolation between the point samples and extrapolation in the unmeasured

540   zones are performed on a physical basis. Both the vertical and lateral integrations allow the computation of the suspended-sand concentration for each ADCP grid cell and consequently the suspended-sand flux.

     The toolbox presented in this article proposes a major advance in the estimation of the uncertainty in point suspended-sand sampling. It addresses several sources of error and integrates existing methods with novel approaches to propose an applicable

framework. The main error sources are identified as u_m due to lateral integration and u_p due to vertical integration, thereby
545   justifying the SDC method, which seeks to improve spatial integration in the whole cross-section.

The application of the methodology on several cross-sectional suspended-sand measurements conducted following different
sampling protocols on four global rivers yields results that slightly differ from the ISO method (-15.9 % to +2.9 % suspended-
sand flux difference). This approach can be easily used and is adaptable to different sampling cases; the only requirement is
an ADCP discharge measurement including several transects and a point samples dataset. The data processing, analysis and
550   visualization toolbox is open-access and available online.

Future development should focus on the incorporation of the acoustic backscatter measured by the ADCP to guide the
vertical and lateral integration, and on the development of more robust methods of estimating the uncertainties due to lateral
integration, the sampler performance and the natural fluctuations in concentration arising from turbulence.

Author contribution

555   GD, JL, JLC, BC conceptualized this work. The methodology was developed by GD, JL, JLC and BC. The code and uncertainty
part was wrote by JL and BCal. GD and JL wrote the original draft of this paper, which was edited by DT, JLC, BCal and BC.
JLC and BC supervised the work. All authors brought ideas into the work, participated on the field measurements and reviewed
the final draft.

Data availability

560   Data are available on: https://doi.org/10.57745/NLFT7Q and https://doi.org/10.57745/YTCYSX.

Code availability

The open-source toolbox is available at: https://gitlab.irstea.fr/jessica.laible/analysis-solid-gauging.

Acknowledgements

The authors thank Thibault Vassor and Alexis Pavaux for their help in this project and Janna Stepanian (INRAE) for her help
565   in the sample analysis. Thanks to K. Spicer (USGS) for sharing data. Thanks to Dr. Benjamin Renard for his valuable help
and review of the uncertainty part. Thanks to the Plan Loire and Stephane Rodrigues from Tours University for lending us the
US-P06 sampler.

Statements and Declarations

Funding for the work was provided by the Compagnie Nationale du Rhône (CNR), Electricité de France (EDF), European
570   Regional Development Fund (ERDF), Agence de l'eau RMC, and three regional councils (Auvergne-Rhône-Alpes, PACA and
Occitanie) in the context of the Rhône Sediment Observatory (OSR, http://www.graie.org/osr). The authors declare no conflict
of interest.

References

575   Armijos, E., Crave, A., Espinoza, R., Fraizy, P., Santos, A. D., Sampaio, F., De Oliveira, E., Santini, W., Martinez, J., Autin, P., Pantoja, N., Oliveira, M., and Filizola, N.: Measuring and modeling vertical gradients in suspended sediments in the Solimões /Amazon River, Hydrological Processes, 31, 654–667, https://doi.org/10.1002/hyp.11059, 2017.

ASTM D3977: Standard test method for determining sediment concentration in water samples., ASTM International, p. 6p, 2007.

Boldt, J. A.: From mobile ADCP to high-resolution SSC: a cross-section calibration tool, in: 3rd Joint Federal Interagency Conference on
580   Sedimentation and Hydrologic Modeling, pp. 1258–1260, Reno, Nevada, 2015.

Bouchez, J., Métivier, F., Lupker, M., Maurice, L., Perez, M., Gaillardet, J., and France-Lanord, C.: Prediction of depth-integrated fluxes of suspended sediment in the Amazon River: Particle aggregation as a complicating factor, Hydrological processes, 25, 778–794, https://doi.org/10.1002/hyp.7868, 2011.

Camenen, B.: Simple and general formula for the settling velocity of particles, Journal of Hydraulic Engineering, 133, 229–233, 2007.

585   Camenen, B. and Larson, M.: A unified sediment transport formulation for coastal inlet application, Tech. rep., US Army Corps of Engineers, Engineer Research and Development Center, 2007.

Camenen, B. and Larson, M.: A general formula for noncohesive suspended sediment transport, Journal of Coastal Research, 24, 615–627, 2008.

Camenen, B., Holubova, K., Lukac, M., Le Coz, J., and Paquier, A.: Assessment of Methods Used in 1D Models for Comput-
590   ing Bed-Load Transport in a Large River: The Danube River in Slovakia, Journal of Hydraulic Engineering, 137, 1190–1199, https://doi.org/10.1061/(ASCE)HY.1943-7900.0000427, 2011.

Camenen, B., Le Coz, J., Dramais, G., Peteuil, C., Fretaud, T., Falgon, A., Dussouillez, P., and Moore, S.: A simple physically-based model for predicting sand transport dynamics in the Lower Mekong River, in: River Flow 2014, pp. 2189–2197, CRC Press, 2014.

Camenen, B., Dramais, G., Laible, J., Le Coz, J., Pierrefeu, G., and Lauters, F.: Quantification of continuous sand flux time-series downstream
595   of a dam during a flushing event, Environmental Fluid Mechanics, (accepted), 2023.

Colby, B.: Discharge of sands and mean-velocity relationships in sand-bed streams, Tech. rep., USGS, 1964.

Delile, H., Masson, M., Miège, C., Le Coz, J., Poulier, G., Le Bescond, C., Radakovitch, O., and Coquery, M.: Hydro-climatic drivers of land-based organic and inorganic particulate micropollutant fluxes: The regime of the largest river water inflow of the Mediterranean Sea, Water Research, 185, 116 067, https://doi.org/10.1016/j.watres.2020.116067, 2020.

600   Despax, A., Le Coz, J., Hauet, A., Mueller, D. S., Engel, F. L., Blanquart, B., Renard, B., and Oberg, K. A.: Decomposition of Uncertainty Sources in Acoustic Doppler Current Profiler Streamflow Measurements Using Repeated Measures Experiments, Water Resources Research, https://doi.org/10.1029/2019WR025296, 2019.

Despax, A., Le Coz, J., Mueller, D. S., Hauet, A., Calmel, B., Pierrefeu, G., Naudet, G., Blanquart, B., and Pobanz, K.: Validation of an Uncertainty Propagation Method for Moving-Boat Acoustic Doppler Current Profiler Discharge Measurements, Water Resources Research,
605   59, https://doi.org/10.1029/2021WR031878, 2023.

Dominguez Ruben, L., Szupiany, R., Latosinski, F., C., L. W., Wood, M., and Boldt, J.: Acoustic Sediment Estimation Toolbox (ASET): A software package for calibrating and processing TRDI ADCP data to compute suspended-sediment transport in sandy rivers, Computers & Geosciences, p. 104499, https://doi.org/10.1016/j.cageo.2020.104499, 2020.

Dramais, G.: Observation et modélisation des flux de sable dans les grands cours d'eau, Ph.D. thesis, University of Lyon, 2020.

610   Filizola, N., Seyler, F., Mourão, M. H., Arruda, W., Spínola, N., and Guyot, J. L.: Study of the variability in suspended sediment discharge at
Manacapuru, Amazon River, Brazil, Latin American journal of sedimentology and basin analysis, 16, 93–99, 2009.

FISP: Laboratory investigation of suspended-sediment samplers, Tech. Rep. Report No. 5, Federal Interagency Sedimentation Project, 1941.

FISP: The design of improved types of suspended sediment samplers, Tech. Rep. Report No. 6, Federal Interagency Sedimentation Project,
1952.

615   Gitto, A. B., Venditti, J. G., Kostaschuk, R., and Church, M.: Representative point-integrated suspended sediment sampling in rivers, Water
Resources Research, 53, 2956–2971, https://doi.org/10.1002/2016WR019187, 2017.

Gordon, J. D.: US Geological Survey Quality-assurance Project for Sediment Analysis, Tech. rep., USGS, 2000.

Gordon, J. D., Newland, C. A., and Gagliardi, S. T.: Laboratory Performance in the Sediment Laboratory Quality-assurance Project, 1996–98,
Water-Resources Investigations Report, 99, 4184, 2000.

620   Grams, P. E., Schmidt, J. C., Wright, S. A., Topping, D., Melis, T. S., and Rubin, D. M.: Building sandbars in the Grand Canyon, Eos, Earth
and Space Science News, 96, 1–11, https://doi.org/10.1029/2015EO030349, 2015.

Gray, J. and Gartner, J.: Overview of selected surrogate technologies for high-temporal resolution suspended sediment monitoring, in: Pro-
ceedings of the 2nd Joint Federal Interagency Conference (June 27–July 1) Las Vegas, NV, USA, Citeseer, 2010.

Gualtieri, C., Angeloudis, A., Bombardelli, F., Jha, S., and Stoesser, T.: On the values for the turbulent Schmidt number in environmental
625   flows, Fluids, 2, 17, https://doi.org/10.3390/fluids2020017, 2017.

Guy, H. P. and Norman, V. W.: Field methods for measurement of fluvial sediment, United State Geological Survey, Book 3, 1970.

Hoffmann, T., Thorndycraft, V., Brown, A., Coulthard, T., Damnati, B., Kale, V., Middelkoop, H., Notebaert, B., and Walling, D.: Human
impact on fluvial regimes and sediment flux during the Holocene: Review and future research agenda, Global and Planetary Change, 72,
87–98, https://doi.org/10.1016/j.gloplacha.2010.04.008, 2010.

630   Hunt, J.: On the turbulent transport of a heterogeneous sediment, The Quarterly Journal of Mechanics and Applied Mathematics, 22, 235–246,
1969.

ISO 4363: Measurement of liquid flow in open channels. Methods for measurement of characteristics of suspended sediment., International
Organization for Standardization, Geneva, Switzerland, 2002.

ISO 748: Hydrometry. Measurement of liquid flow in open channels using current-meters or floats using point velocity measurements.,
635   International Organization for Standardization, Geneva, Switzerland, p. 46 p, 2009.

JCGM: Evaluation of measurement data - Guide to the expression of uncertainty in measurement - JCGM, ISO, 50, 134, 2008.

Khodashenas, S. R. and Paquier, A.: A geometrical method for computing the distribution of boundary shear stress across irregular straight
open channels, Journal of Hydraulic Research, 37, 381–388, 1999.

Kondolf, G. M.: Hungry water: effects of dams and gravel mining on river channels, Environmental management, 21, 533–551, 1997.

640   Kondolf, G. M., Gao, Y., Annandale, G. W., Morris, G. L., Jiang, E., Zhang, J., Cao, Y., Carling, P., Fu, K., Guo, Q., et al.: Sustainable
sediment management in reservoirs and regulated rivers: Experiences from five continents, Earth's Future, 2, 256–280, 2014.

Lennermark, M. and Hauet, A.: Developing a post-processing software for ADCP discharge measurement piloted by an international and
inter-agency group: a unique, ambitious experience... and one that works!, in: EGU General Assembly 2022, Vienna, Austria, EGU22-
9379, https://doi.org/10.5194/egusphere-egu22-9379, 2022.

645   Lupker, M., France-Lanord, C., Lavé, J., Bouchez, J., Galy, V., Métivier, F., Gaillardet, J., Lartiges, B., and Mugnier, J.: A Rouse-based
method to integrate the chemical composition of river sediments: Application to the Ganga basin, Journal of Geophysical Research: Earth
Surface, 116, 1–24, https://doi.org/10.1029/2010JF001947, 2011.

Mansanarez, V., Renard, B., Le Coz, J., Lang, M., and Darienzo, M.: Shift Happens! Adjusting Stage-Discharge Rating Curves to Morphological Changes at Known Times, Water Resources Research, 55, 2876–2899, https://doi.org/10.1029/2018WR023389, 2019.

650 McLean, S.: On the calculation of suspended load for noncohesive sediments, Journal of Geophysical Research: Oceans, 97, 5759–5770, 1992.

Mueller, D. S.: QRev-Software for computation and quality assurance of acoustic Doppler current profiler moving-boat streamflow measurements, US Geological Survey Open-File Report, 1052, 50, https://doi.org/10.3133/ofr20161068, technical manual for version 2.8, 2016.

655 Némery, J., Mano, V., Coynel, A., Etcheber, H., Moatar, F., Meybeck, M., Belleudy, P., and Poirel, A.: Carbon and suspended sediment transport in an impounded alpine river (Isère, France), Hydrological Processes, 27, 2498–2508, https://doi.org/https://doi.org/10.1002/hyp.9387, 2013.

Oberg, K. and Mueller, D. S.: Validation of streamflow measurements made with acoustic Doppler current profilers, Journal of Hydraulic Engineering, 133, 1421–1432, https://doi.org/10.1061/(ASCE)0733-9429(2007)133:12(1421, 2007.

660 Parsons, D. R., Jackson, P., Czuba, J., Engel, F., Rhoads, B. L., Oberg, K., Best, J. L., Mueller, D., Johnson, K., and Riley, J.: Velocity Mapping Toolbox (VMT): a processing and visualization suite for moving-vessel ADCP measurements, Earth Surface Processes and Landforms, 38, 1244–1260, https://doi.org/10.1002/esp.3367, 2013.

Perret, E., Camenen, B., Berni, C., El kadi Abderrezzak, K., and Renard, B.: Uncertainties in Models Predicting Critical Bed Shear Stress of Cohesionless Particles, Journal of Hydraulic Engineering, 149, 04023 002, 2023.

665 Porterfield: Computation of fluvial-sediment discharge, techniques of water-resources investigations 03-c3 edn., https://doi.org/10.3133/twri03C3, 1972.

Poulier, G., Launay, M., Le Bescond, C., Thollet, F., Coquery, M., and Le Coz, J.: Combining flux monitoring and data reconstruction to establish annual budgets of suspended particulate matter, mercury and PCB in the Rhône River from Lake Geneva to the Mediterranean Sea, Science of the Total Environment, 658, 457–473, https://doi.org/10.1016/j.scitotenv.2018.12.075, 2019.

670 Renard, B., Garreta, V., and Lang, M.: An application of Bayesian analysis and Markov chain Monte Carlo methods to the estimation of a regional trend in annual maxima, Water resources research, 42, https://doi.org/10.1029/2005WR004591, 2006.

Rouse, H.: Modern conceptions of the mechanics of fluid turbulence, Trans ASCE, 102, 463–505, 1937.

Sabol, T. A. and Topping, D. J.: Evaluation of intake efficiencies and associated sediment-concentration errors in US D-77 bag-type and US D-96-type depth-integrating suspended-sediment samplers, US Geological Survey Scientific Investigations Report 2012-5208, 88 p.,

675 5208, 88, https://doi.org/10.3133/sir20125208, 2013.

Santini, W., Camenen, B., Le Coz, J., Vauchel, P., Guyot, J.-L., Lavado, W., Carranza, J., Paredes, M. A., Pérez Arévalo, J. J., Arévalo, N., Espinoza Villar, R., Julien, F., and Martinez, J.-M.: An index concentration method for suspended load monitoring in large rivers of the Amazonian foreland, Earth Surface Dynamics, 7, 515–536, https://doi.org/10.5194/esurf-7-515-2019, 2019.

Shah-Fairbank, S. C. and Julien, P. Y.: Sediment load calculations from point measurements in sand-bed rivers, International Journal of

680 Sediment Research, 30, 1–12, https://doi.org/10.1016/S1001-6279(15)60001-4, 2015.

Smart, G.: A base for the log law and von Karman's constant problem, Journal of Hydraulic Research, 60, 935–943, https://doi.org/10.1080/00221686.2022.2076164, 2022.

Soulsby, R., Whitehouse, R., et al.: Threshold of sediment motion in coastal environments, in: Pacific Coasts and Ports' 97: Proceedings of the 13th Australasian Coastal and Ocean Engineering Conference and the 6th Australasian Port and Harbour Conference; Volume 1, p.

685 145, Centre for Advanced Engineering, University of Canterbury, 1997.

Spicer, K.: P-6 Comparison Tests. A Point-Integrating Suspended Sediment Sampler Comparison, SEDHYD Conference, 2019.

Starosolsky, O. and Rakoczi, L.: Operational hydrology report (OHR), 16. Measurement of river sediments : prepared by the Rapporteur on Sediment Transport of the Commission for Hydrology, World Meteorological Organisation, 1981.

Szupiany, R. N., Lopez Weibel, C., Guerrero, M., Latosinski, F., Wood, M., Dominguez Ruben, L., and Oberg, K.: Estimating sand concentrations using ADCP-based acoustic inversion in a large fluvial system characterized by bi-modal suspended-sediment distributions, Earth Surface Processes and Landforms, 44, 1295–1308, https://doi.org/10.1002/esp.4572, 2019.

Topping, D. J. and Wright, S. A.: Long-term continuous acoustical suspended-sediment measurements in rivers - Theory, application, bias, and error, US Geological Survey Professional Paper 1823, 98 p., https://doi.org/10.3133/pp1823, 2016.

Topping, D. J., Rubin, D. M., Wright, S. A., and Melis, T. S.: Field evaluation of the error arising from inadequate time averaging in the standard use of depth-integrating suspended-sediment samplers, US Geological Survey Professional Paper 1774, 95 p., 2011.

Van Rijn, L. C.: Sediment transport, part II: suspended load transport, Journal of hydraulic engineering, 110, 1613–1641, 1984.

Vauchel, P., Santini, W., Guyot, J. L., Moquet, J. S., Martinez, J. M., Espinoza, J. C., Baby, P., Fuertes, O., Noriega, L., Puita, O., et al.: A reassessment of the suspended sediment load in the Madeira River basin from the Andes of Peru and Bolivia to the Amazon River in Brazil, based on 10 years of data from the HYBAM monitoring programme, Journal of Hydrology, 553, 35–48, https://doi.org/10.1016/j.jhydrol.2017.07.018, 2017.

Venditti, J., Church, M., Attard, M., and Haught, D.: Use of ADCPs for suspended sediment transport monitoring: An empirical approach, Water Resources Research, 52, 2715–2736, https://doi.org/10.1002/2015WR017348, 2016.

Vergne, A., Le Coz, J., Berni, C., and Pierrefeu, G.: Using a Down-Looking Multifrequency ABS for Measuring Suspended Sediments in Rivers, Water Resources Research, 56, e2019WR024 877, https://doi.org/10.1029/2019WR024877, 2020.

Vergne, A., Le Coz, J., and Berni, C.: Some Backscatter Modeling Issues Complicating the Sonar-Based Monitoring of Suspended Sediments in Rivers, Water Resources Research, 59, https://doi.org/10.1029/2022WR032341, 2023.

Wren, D., Barkdoll, B., Kuhnle, R., and Derrow, R.: Field techniques for suspended-sediment measurement, Journal of Hydraulic Engineering, 126, 97–104, https://doi.org/10.1061/(ASCE)0733-9429(2000)126:2(97), 2000.